Article

Current Biology

Spaced training activates Miro/Milton-dependent mitochondrial dynamics in neuronal axons to sustain long-term memory

Graphical abstract

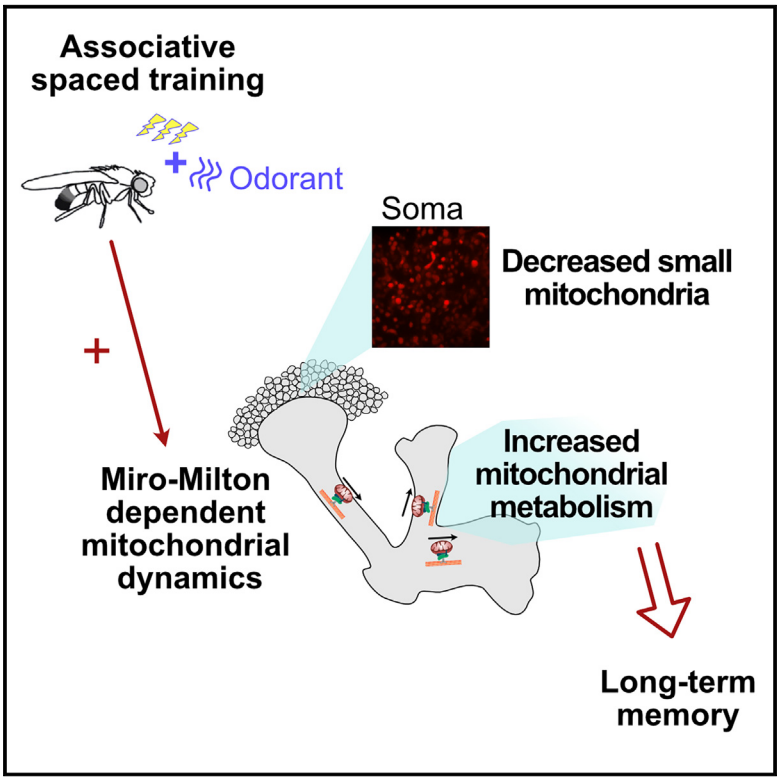

Highlights

- Miro-Milton-dependent mitochondria dynamics in mushroom body neurons sustain LTM
- Small mitochondria are partially depleted from neuronal soma upon LTM formation
- At the same time, mitochondria dynamics are increased in axons
- This increase sustains LTM through axonal upregulation of mitochondria metabolism

Authors

Alice Pavlowsky, Typhaine Comyn, Julia Minatchy, ..., Lydia Danglot, Thomas Preat, Pierre-Yves Plaçais

Correspondence

thomas.preat@espci.fr (T.P.), pierre-yves.placais@espci.fr (P.-Y.P.)

In brief

Pavlowsky et al. investigate *in vivo* the role of mitochondria dynamics in associative olfactory memory. They demonstrate that Miro-Milton mitochondria dynamics are required to sustain the upregulation of axonal mitochondria metabolism specifically needed for long-term memory formation.

Pavlowsky et al., 2024, Current Biology *34*, 1904–1917
May 6, 2024 © 2024 The Authors. Published by Elsevier Inc.
https://doi.org/10.1016/j.cub.2024.03.050

CellPress

CellPress
OPEN ACCESS

Current Biology

Article

Spaced training activates Miro/Milton-dependent mitochondrial dynamics in neuronal axons to sustain long-term memory

Alice Pavlowsky,[1] Typhaine Comyn,[1] Julia Minatchy,[1] David Geny,[2] Philippe Bun,[2] Lydia Danglot,[2] Thomas Preat,[1,*] and Pierre-Yves Plaçais[1,3,*]
[1]Energy & Memory, Brain Plasticity Unit, CNRS, ESPCI Paris, PSL Research University, 10 rue Vauquelin, 75005 Paris, France
[2]Université de Paris, NeurImag Imaging Facility, Institute of Psychiatry and Neuroscience of Paris, INSERM U1266, 75014 Paris, France
[3]Lead contact
*Correspondence: thomas.preat@espci.fr (T.P.), pierre-yves.placais@espci.fr (P.-Y.P.)
https://doi.org/10.1016/j.cub.2024.03.050

SUMMARY

Neurons have differential and fluctuating energy needs across distinct cellular compartments, shaped by brain electrochemical activity associated with cognition. *In vitro* studies show that mitochondria transport from soma to axons is key to maintaining neuronal energy homeostasis. Nevertheless, whether the spatial distribution of neuronal mitochondria is dynamically adjusted *in vivo* in an experience-dependent manner remains unknown. In *Drosophila*, associative long-term memory (LTM) formation is initiated by an early and persistent upregulation of mitochondrial pyruvate flux in the axonal compartment of neurons in the mushroom body (MB). Through behavior experiments, super-resolution analysis of mitochondria morphology in the neuronal soma and *in vivo* mitochondrial fluorescence recovery after photobleaching (FRAP) measurements in the axons, we show that LTM induction, contrary to shorter-lived memories, is sustained by the departure of some mitochondria from MB neuronal soma and increased mitochondrial dynamics in the axonal compartment. Accordingly, impairing mitochondrial dynamics abolished the increased pyruvate consumption, specifically after spaced training and in the MB axonal compartment, thereby preventing LTM formation. Our results thus promote reorganization of the mitochondrial network in neurons as an integral step in elaborating high-order cognitive processes.

INTRODUCTION

Mitochondria perform central functions in neuronal physiology, such as ATP production via oxidative phosphorylation, Ca^{2+} buffering, redox regulation, and synthesis of neurotransmitter precursors.[1–6] In addition, mitochondria form a highly dynamic network of organelles that continuously move, fuse, and divide.[7] This morphological plasticity allows for adjusting mitochondrial functions to the specific needs of the different cellular compartments.[8] This is of particular importance in neurons, which are highly polarized cells composed of three different structural and functional domains: the cell body or soma, the dendrites, and the axon. In neuronal soma and dendrites, mitochondria form an extensively connected and dynamic network, whereas they are mostly found in a singular state in the axon.[8] Although the soma is the main site of mitochondria biogenesis, other areas, such as the axonal presynaptic terminals or postsynaptic dendrites, are in high demand of mitochondria activity for energy supply and Ca^{2+} buffering.[9,10] Numerous *in vitro* studies show that maintaining energy homeostasis throughout the neuron requires efficient delivery of mitochondria from the soma to distal areas such as the axonal terminals.[8,11] This involves both long-range transport of mitochondria along the axon, which is driven by microtubule-based dynein and kinesin motors, and local mitochondria movement and anchoring at the presynaptic site or in the dendritic spine, driven by actin-based myosin motors.[10] Although there is extensive literature describing how mitochondrial dynamics and, in particular, mitochondria motility are critical for synaptic plasticity *in vitro*,[12–17] it has never been confirmed *in vivo* that mitochondria motility across neuronal compartments is required to meet the acute increases in energy demand imposed by challenging brain tasks such as memory formation. Nevertheless, there is a strong need to better incorporate the role of mitochondrial transport in an integrated description of major brain functions, since the disruption of mitochondria axonal transport has been linked to several neurodegenerative conditions.[18–21]

The main actors of mitochondrial dynamics, and in particular of long-range axonal transport, are conserved across species.[22] Thus, identification of the molecular adapters Milton and Miro, which couple microtubule-based motor proteins to mitochondria, came from genetic screens for synaptic insufficiency in *Drosophila melanogaster*.[23–26] Milton interacts directly with either the kinesin heavy chain (Khc) or the dynactin-dynein complex, which respectively convey mitochondria anterogradely or retrogradely[23,24,26–28] (Figure 1A). In addition, Milton is localized to the mitochondria via its binding to Miro, a mitochondrial Rho GTPase protein attached to the outer mitochondrial

 © 2024 The Authors. Published by Elsevier Inc.
This is an open access article under the CC BY-NC-ND license (http://creativecommons.org/licenses/by-nc-nd/4.0/).

CellPress
OPEN ACCESS

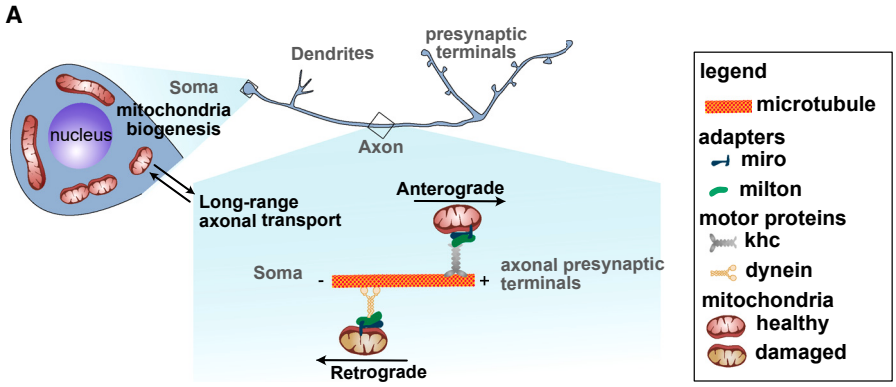

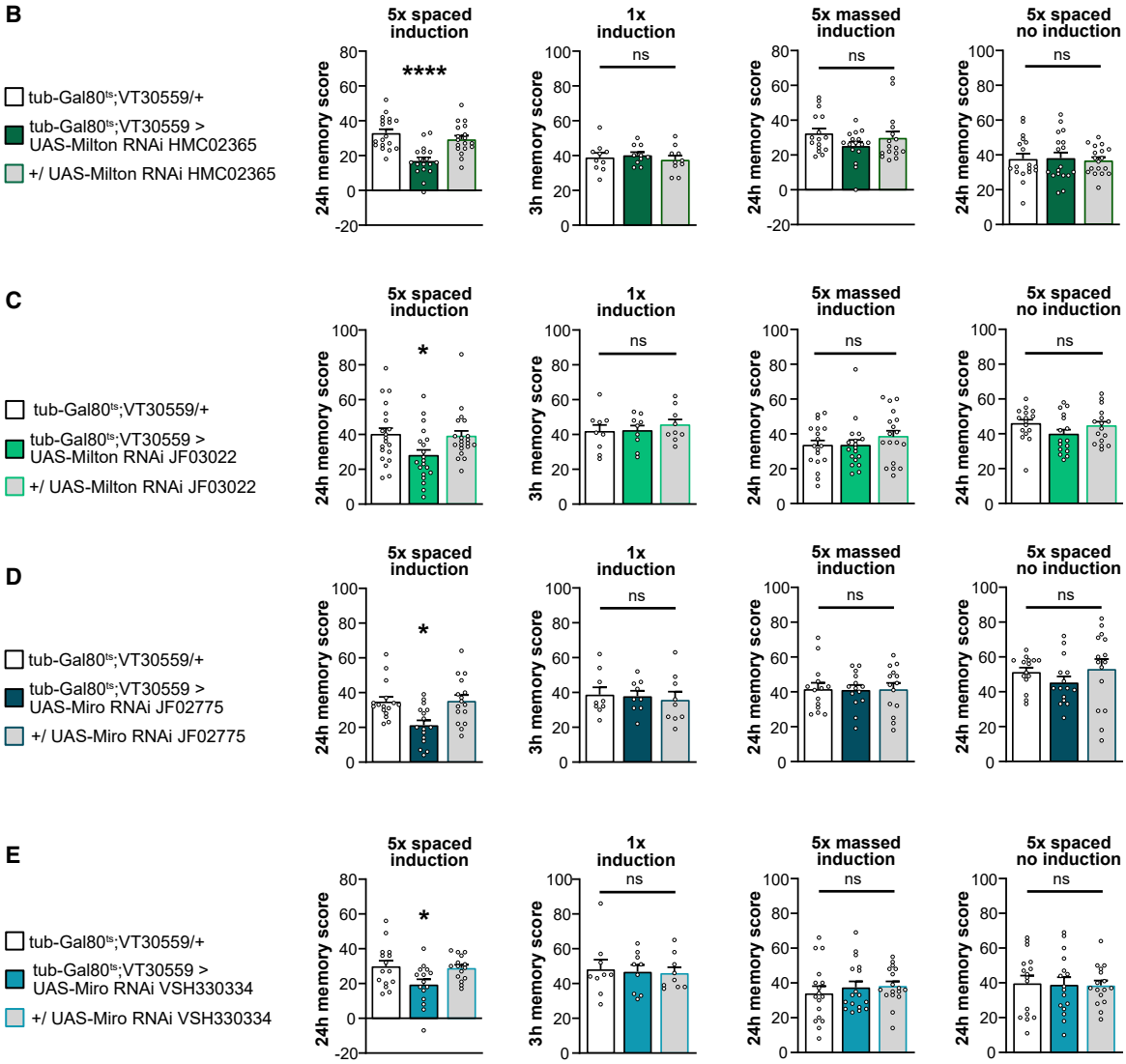

(legend on next page)

membrane.[25,29,30] At the behavioral level, *Drosophila* display elaborate olfactory associative memory processes involving defined and well-described neuronal networks belonging to a specific brain structure, the mushroom body (MB).[31–33] We previously demonstrated that formation of associative aversive long-term memory (LTM) requires the upregulation, following learning, of mitochondrial metabolism in MB neurons, occurring at least in the axonal compartment.[34] However, the cellular mechanisms supporting this upregulation of mitochondrial metabolism upon LTM establishment are currently unknown.

Here, we used a combination of behavioral experiments involving genetic knockdown (KD) in adult flies, characterization of mitochondrial morphology in MB soma with unprecedented detail using super-resolution 3D-stimulated emission depletion (3D-STED) microscopy, *in vivo* measurements of axonal mitochondrial dynamics in MB neurons, and *in vivo* imaging of pyruvate metabolism in different compartments of MB neurons. We found that Miro and Milton are required specifically for LTM but not for shorter-lasting associative memory. We revealed that LTM training induces a partial depletion of small mitochondria in the soma compartment of MB neurons, while in the axonal compartment, it triggers an increase in mitochondrial dynamics, and we showed that both processes are dependent on Miro and Milton. Finally, we demonstrated that upregulation of mitochondrial metabolism upon LTM formation is dependent on Miro and Milton in the axonal compartment of MB neurons but not in the other compartments such as the dendrites and the soma. Overall, we show that mitochondria motility is required to meet the increase in metabolic demand in the axonal compartment imposed by LTM formation.

RESULTS

Miro-Milton-dependent mitochondrial dynamics are specifically required for LTM

Drosophila can form associative aversive olfactory memory as a result of the association between an odorant and electric shocks, which is stored in Kenyon cells (KCs), the intrinsic neurons of the MB.[32,35,36] Stimulation of the olfactory pathway by a pure odorant sparsely activates a small fraction of the whole KC population.[37] After experiencing a single cycle of conditioning—the sequential presentation of two odorants, one of which is paired with electric shocks—flies form a memory that decays within hours.[38,39] After a spaced training—5 repeated cycles of conditioning, spaced by 15-min rest intervals—flies form a robust memory that can persist for several days.[38,40] At the circuit level, starting around 14 h after spaced training, it arguably mobilizes the parallel retrieval of two components that are separately encoded within MB networks.[41] However, memory after spaced training (hereafter LTM) was fully abolished by MB KD of the mitochondrial pyruvate transporter MPC1,[42] and forming LTM imposes an acute metabolic challenge on MB neurons.[34] By contrast, when flies are exposed to a massed training (i.e., 5 repetitions of training cycle without any rest intervals), the memory formed lasts for around 24 h[35] but is independent from mitochondria pyruvate metabolism.[34,42] To investigate the role of transport of mitochondria in response to energy demand upon LTM formation, we downregulated in adult MB neurons Milton and Miro, the adapters mediating microtubule-based mitochondria transport, but not the microtubule-based motor proteins, to avoid targeting the axonal transport of organelles in general. To restrict the expression of Milton RNAi to adult MB neurons, we used the VT30559-Gal4 driver in combination with a ubiquitously expressed thermosensitive Gal4 inhibitor, Gal80 (tub-Gal80^{ts}),[43] so that GAL4 transcriptional activity could be induced by placing flies at 30°C for 3 days. Following spaced training, LTM was impaired by downregulating Milton expression in adult MB neurons, whereas after a single-cycle training, memory tested at 3 h (3-h memory) was normal, as well as 24-h memory after massed training (Figure 1B) (male and female flies were used indiscriminately in all behavior experiments). LTM was normal in a control experiment where flies were not subjected to heat activation and thus deprived of RNAi expression (Figure 1B). Finally, shock reactivity and olfactory acuity controls were normal in induced flies (Table 1). To test whether Milton KD specifically affects late-forming memory after spaced training,[41] we investigated the time course of memory decay. 3 h after spaced training, memory was not affected by Milton KD, whereas 8 h after training, memory performance started to decrease as compared with genotypic controls, without reaching significance (Figure S1A). 16 h after spaced training, Milton KD in adult MB neurons resulted in a significant memory defect (Figure S1A), as observed 24 h after training (classical LTM measurement, Figure 1B). These results show that Milton is required specifically for late-forming memory after spaced training. Using a second non-overlapping Milton RNAi, we confirmed that Milton

Figure 1. Miro-Milton-dependent mitochondrial dynamics in MB are required specifically for LTM

(A) Schema of mitochondria transport in a typical MB *Drosophila* neuron. The soma is the main place of mitochondria biogenesis and contains large mitochondria. To travel from the soma to the sites in high demand of mitochondria such as the presynaptic terminals, small mitochondria are transported along microtubules. Transport of mitochondria requires the adapter proteins Miro and Milton to anchor mitochondria on the motor proteins khc or dynein.

(B) Milton knockdown (KD) in adult MB neurons impaired memory after spaced training (n = 18, $F_{2,51}$ = 16.30, p < 0.0001), but not after one-cycle training (n = 10, $F_{2,27}$ = 0.32, p = 0.73) or massed training (n = 16, $F_{2,45}$ = 1.55, p = 0.22). Without induction of Milton RNAi, memory after spaced training was normal (n = 18, $F_{2,51}$ = 0.06, p = 0.94).

(C) Similar results were obtained using a second non-overlapping RNAi against Milton: memory defect after spaced training (n = 20, $F_{2,57}$ = 3.78, p = 0.029), but not after one-cycle training (n = 9, $F_{2,24}$ = 0.36, p = 0.70) or massed training (n = 18, $F_{2,51}$ = 0.81, p = 0.44) or without RNAi induction (n = 16, $F_{2,45}$ = 1.54, p = 0.22).

(D) Miro KD in adult MB neurons impaired memory after spaced training (n = 16, $F_{2,45}$ = 7.39, p = 0.0017), but not after one-cycle training (n = 9, $F_{2,24}$ = 0.15, p = 0.87) or massed training (n = 14, $F_{2,39}$ = 0.006, p = 0.99). Without induction of Miro RNAi, memory after spaced training was normal (n = 15, $F_{2,42}$ = 1.00, p = 0.37).

(E) Similar results were obtained using a second non-overlapping RNAi against Miro: memory defect after spaced training (n = 15, $F_{2,42}$ = 4.43, p = 0.018), but not after one-cycle training (n = 9, $F_{2,24}$ = 0.067, p = 0.94) or massed training (n = 17, $F_{2,48}$ = 0.43, p = 0.65) or without RNAi induction (n = 16, $F_{2,45}$ = 0.024, p = 0.98).

Bar plots: mean ± SEM with dots as individual values, one-way ANOVA with post hoc testing by the Newman-Keuls pairwise comparisons test. p value of the pairwise comparison test: * p < 0.05, **** p < 0.0001, ns, not significant, p > 0.05. See Table 1 for sensory acuity controls and see also Figure S1.

CellPress
OPEN ACCESS

Table 1. Sensory acuity controls

			Naive odor avoidance			
	Shock avoidance		Octanol		Methylcyclohexanol	
Genotypes	Mean ± SEM	Statistics	Mean ± SEM	Statistics	Mean ± SEM	Statistics
tubGal80^{ts};VT30559/+	53.3 ± 5.3	$F_{2,39}$ = 4.5, p = 0.017[a], n = 14	60.8 ± 4.2	$F_{2,45}$ = 1.1	65.4 ± 4.6	$F_{2,45}$ = 0.88
tubGal80^{ts}; VT30559>, UAS-Milton RNAi HMC02365	60.9 ± 5.2		68.1 ± 4.9	p = 0.33	74.2 ± 4.3	p = 0.42
UAS-Milton RNAi HMC02365/+	74.2 ± 4.4		58.6 ± 4.9	n = 16	67.4 ± 5.8	n = 16
tubGal80^{ts};VT30559/+	58.9 ± 7.6	$F_{2,39}$ = 0.57, p = 0.57, n = 14	55.8 ± 4.4	$F_{2,33}$ = 0.68	49.3 ± 5.1	$F_{2,45}$ = 0.83
tubGal80^{ts};VT30559>, UAS-Milton RNAi JF03022	52.3 ± 5.2		52.6 ± 4.9	p = 0.51	57.9 ± 5.0	p = 0.44
UAS-Milton RNAi JF03022/+	50.0 ± 5.1		47.1 ± 6.5	n = 12	50.8 ± 5.0	n = 16
tubGal80^{ts};VT30559/+	54.0 ± 6.6	$F_{2,33}$ = 0.18, p = 0.83, n = 12	54.3 ± 4.8	$F_{2,26}$ = 0.80	48.9 ± 7.3	$F_{2,27}$ = 0.11
tubGal80^{ts};VT30559>, UAS-Miro RNAi JF02775	58.0 ± 6.9		46.4 ± 4.6	p = 0.46	50.8 ± 6.3	p = 0.89
UAS-Miro RNAi JF02775/+	59.3 ± 5.5		54.6 ± 6.3	n = 9–10	46.8 ± 3.7	n = 10
tubGal80^{ts};VT30559/+	44.9 ± 3.5	$F_{2,45}$ = 0.96, p = 0.39, n = 16	63.8 ± 4.8	$F_{2,45}$ = 0.24	57.7 ± 3.7	$F_{2,45}$ = 0.20
tubGal80^{ts}; VT30559>, UAS-Miro RNAi VSH330334	48.4 ± 2.9		63.6 ± 3.8	p = 0.79	53.9 ± 4.2	p = 0.82
UAS-Miro RNAi VSH330334/+	41.8 ± 3.6		60.3 ± 3.5	n = 16	56.8 ± 5.2	n = 16

[a]Newman-Keuls post hoc comparison between genotype of interest and controls are not significant: tubGal80^{ts}; VT30559>UAS-Milton RNAi HMC02365 vs. tubGal80^{ts}; VT30559/+: ns. tubGal80^{ts}; VT30559>UAS-Milton RNAi HMC02365 vs. UAS-Milton RNAi HMC02365/+: ns. tubGal80^{ts}; VT30559/+ vs. UAS-Milton RNAi HMC02365/+: *.

KD specifically impairs memory after spaced training (Figure 1C; Table S1). These two Milton RNAi lines have been used previously to efficiently knock down Milton, both at the molecular level and the functional level.[44–46] Nevertheless using a dsRed addressed to the mitochondria matrix (mt-dsRed) as a mitochondria marker,[47] we observed that after 3 days induction, expression of the Milton RNAi HMC02365 leads to a drastic decrease in mitochondria content in the MB axons of naive flies compared with naive control flies expressing only mt-dsRed (Figures S1B and S1C), as previously described in the wing neurons,[46] whereas 3 days induction of the Milton RNAi JF03022 did not affect the overall distribution of mitochondria as compared with control flies (Figures S1B and S1D). This difference could be due to distinct RNAi efficiencies. The fact that both RNAis induced LTM deficits independently of their effect on the basal mitochondria axonal content suggests that LTM impairment is linked to disruption of training-induced regulations of mitochondrial dynamics rather than defects in basal mitochondrial axonal content. The specific requirement of Milton for LTM prompted us to investigate if it was more particularly required in α/β neurons of the MB, the subpopulation of MB neurons in which LTM is encoded.[35,48,49] We restricted Milton RNAi expression to the α/β neurons and observed a strong LTM defect after spaced training, whereas LTM was normal when RNAi was not induced (Figure S1E). By contrast, when Milton expression was reduced in either of the two other subpopulations of MB neurons, i.e., the α'/β' neurons or the γ neurons,[32] LTM was normal (Figures S1F and S1G, respectively). Altogether, these data reveal that Milton is required in MB α/β neurons specifically for the establishment of LTM.

Next, we investigated if the specific LTM defect was also observed when targeting the other mitochondrial motor adaptor protein, Miro. Indeed, LTM was impaired when Miro was knocked down in adult MB neurons by an RNAi previously used to efficiently downregulate Miro at the functional level,[45,50] whereas 3-h memory after single-cycle training and 24-h memory after massed training were normal (Figure 1D). When RNAi expression was not induced, LTM was not impaired (Figure 1D). Shock reactivity and olfactory acuity controls were normal in induced flies (Table 1). These behavior experiments were replicated using a second non-overlapping Miro RNAi (Figure 1E; Table 1). At the molecular level, both Miro RNAi lines efficiently reduced Miro mRNA level (Figures S1H and S1I). In addition, similar to Milton RNAi JF03022, the expression of either Miro RNAi in adult MB after 3 days of induction did not affect the overall distribution of mitochondria across MB compartments in naive flies (Figures S1J and S1K). Then, as for Milton, we demonstrated that Miro is required in MB α/β neurons specifically for LTM (Figures S1L–S1N). However, in addition to its main function in mitochondria transport, Miro has also been shown to regulate mitochondria fission[51] via interaction with Vimar.[52] Thus, to decipher which functions of Miro are required for LTM, we investigated whether Vimar was required for LTM. KD of Vimar in adult MB neurons did not affect either LTM or 3-h memory after single-cycle training (Figures S1O–S1Q). Altogether, these results demonstrate that in adult MB neurons, both Miro and Milton are necessary for LTM, whereas they are not required to establish other aversive associative olfactory memories.

Upon LTM formation, partial depletion of small mitochondria occurs in MB neuronal soma

We have shown that both Miro and Milton are required specifically for LTM, suggesting that microtubule-mediated mitochondria transport is involved in LTM formation. However,

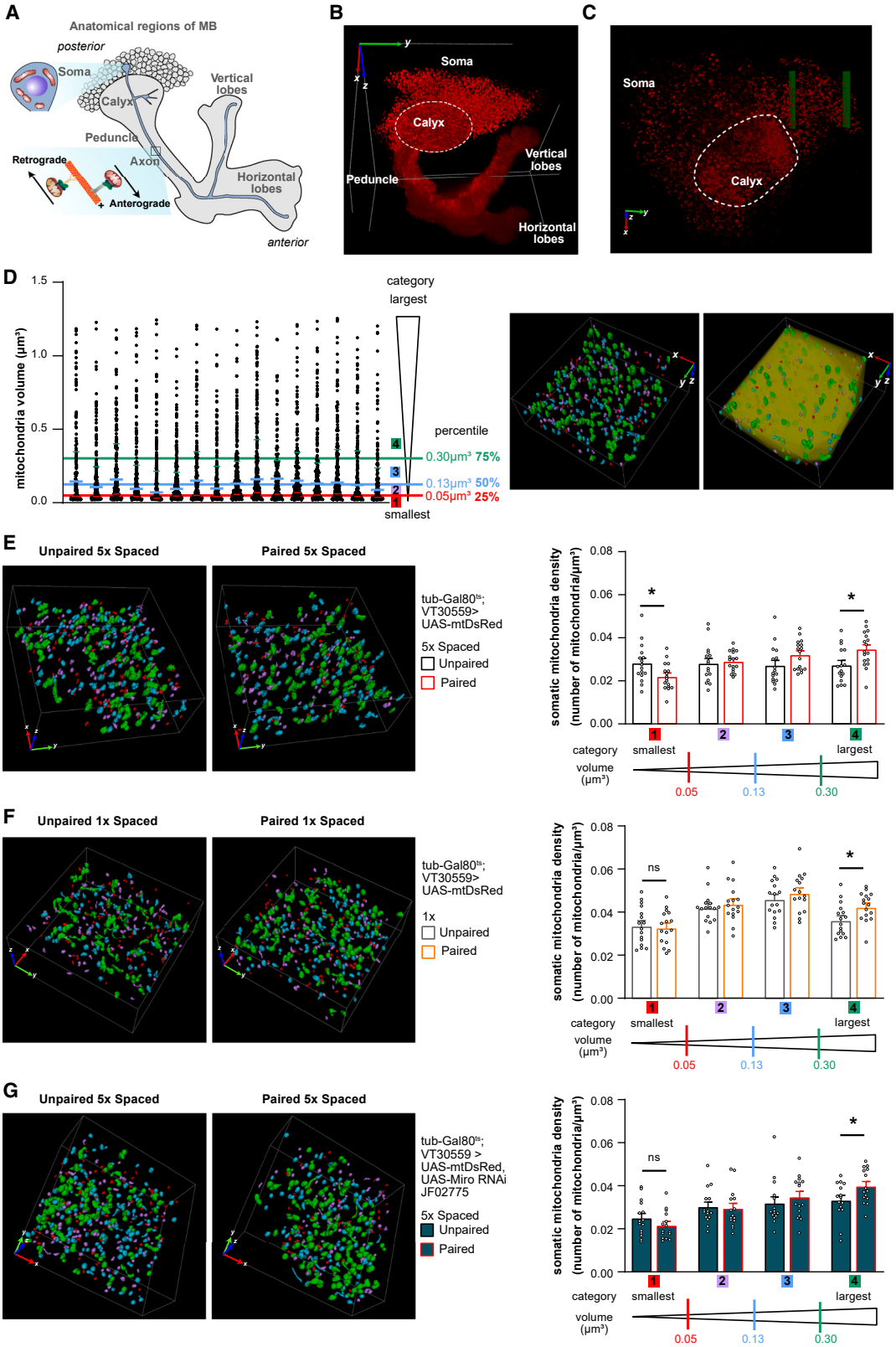

Figure 2. Upon LTM formation, partial depletion of small mitochondria occurs in MB neuronal soma

(A) Schema of MB anatomy (frontal projection view).

(B) Sagittal view of the MB soma region of flies expressing mitochondrial dsRed in MB neurons using confocal microscopy (white dashed line: calyx).

(legend continued on next page)

CellPress
OPEN ACCESS

the Milton-Miro complex mediates bidirectional transport of mitochondria: the anterograde transport from the soma toward the axons in response to energy demand, and the retrograde one for the removal of damaged mitochondria from axons[53] (Figure 1A). As opposed to other *in vivo* models of mitochondria trafficking such as the fly wing axon in which mitochondria movements are in a 2D plan,[54–56] the axons of MB neurons are tightly packed, resulting in a 3D structure known as the lobes (Figures 2A and 2B), where tracking single mitochondria has not been achieved. Mitochondria are highly dynamic organelles, and their morphology is related to their mobility. The mitochondria of axons are mostly present as bean-shaped organelles, a morphological state known to be more mobile than the large, tubular mitochondria that are mainly present in neuronal soma.[12,26,57,58] Thus, to gain insight into ongoing mitochondrial dynamics, we aimed to characterize mitochondria morphology in MB neurons after training. We hypothesized that if spaced training elicits mitochondria trafficking in MB neurons from the soma to the axonal compartment, this would result in the partial depletion of small mitochondria in the soma region. We used 3D-STED super-resolution microscopy to obtain a sufficient spatial resolution for a fine description of the distribution of mitochondria morphology in MB neurons. These are unipolar neurons, with their soma in the posterior part of the brain. Neurites first arborize into a mostly dendritic compartment, forming the calyx. These neurites are then bundled into an axonal fascicle, the peduncle, that traverses the brain posteriorly to anteriorly. In the anterior part of the brain, axons ramify into vertical and horizontal lobes[31] (see also Figures 2A and 2B and Video S1). We imaged the MB in the fixed brains of female flies expressing the mt-dsRed[47] in adult MB neurons (same *Drosophila* line as in Figure S1B). The fiber density and resulting mitochondria concentration were too high in the lobes for single mitochondria to be resolved, even with this super-resolution technique (Figures 2B and 2C; Videos S1 and S2). However, in the soma compartment, we succeeded in separately characterizing the 3D morphology of individual mitochondria (Figure 2D; Video S3). We characterized mitochondria volume distribution and defined four categories of mitochondria based on their volume, ranging from the smallest (category 1) to the largest (category 4) mitochondria. For each brain, we calculated a density of mitochondria for each category (see STAR Methods for details). As our prior work revealed that regulations of energy metabolism involving mitochondria are detectable in the first 2 h after spaced training,[34] we performed the analysis on brains fixed 1 h after training. We did not observe any significant difference in the global mitochondria density between paired and unpaired flies (Figure S2A). However, in flies subjected to spaced associative training, small mitochondria were partially depleted from the soma of MB neurons as compared with experimental control flies, i.e., flies subjected to unpaired non-associative training (Figure 2E; Video S4). The intermediate categories of mitochondria were not significantly affected by associative spaced training, whereas the density of the largest mitochondria was increased (Figure 2E). The increase in the density of the largest mitochondria upon associative training is also reflected by the increase in the total volume of mitochondria upon associative training (Figure S2B). Thus, after spaced training, at a time period when mitochondrial metabolism is upregulated in the axonal compartment of MB neurons, the MB neuronal soma is partially depleted of small mitochondria, and the density of the largest mitochondria is increased. Interestingly, when we performed the same analysis in the dendritic compartment, i.e., the calyx, the densities of the two smallest mitochondria categories were not modified by associative training, whereas the densities of the largest categories were increased (Figures S2C and S2D). These results suggest that the partial depletion of small mitochondria in the soma does not originate from a permanent transfer to the neighboring dendritic compartment.

To assess if any of these changes (either the partial depletion of small mitochondria from the MB neuronal soma or the increase in the large ones) are specific to spaced associative training, we performed the same analysis after single-cycle training. Single-cycle associative training did not induce any significant change in the total density of mitochondria in the soma of MB neurons (Figure S2E). However, it is notable that the total density of mitochondria in the soma after spaced training (Figure S2A) is decreased as compared with the total density of mitochondria after one-cycle training (Figure S2E), suggesting that repeated presentations of odor or reinforcement may globally

(C) View of one entire MB soma region of one brain hemisphere acquired using 3D-STED microscopy.

(D) For each region of interest (ROI) (green box, one per brain), mitochondria were detected and their volume determined. The distribution of mitochondria volume for each ROI of all unpaired control flies used in this work is shown in the graph, where each dot represents the volume of one single identified mitochondrion. The means of the quartile limits from of all spaced unpaired control flies were used to define the 4 categories of mitochondria. A representative ROI sample is shown with a color code corresponding to the 4 mitochondria volume categories (category 1: red, 2: purple, 3: blue, 4: green). We calculated the density of mitochondria for each category using the volume of the minimal envelope containing all of the detected mitochondria in the ROI (right panel: in yellow: the minimal envelope was determined using a custom-written Fiji macro[59]).

(E) 1 h after spaced training, in flies subjected to spaced associative training, small mitochondria were depleted from MB neuronal soma as compared with control flies subjected to unpaired training (smallest mitochondria category, 1: n = 16–17, t_{31} = 2.35, p = 0.025). The intermediate categories (2 and 3) were not significantly affected by associative spaced training (2: n = 16–17, t_{31} = 0.39, p = 0.70; 3: n = 16–17, t_{31} = 1.79, p = 0.084), whereas the density of the largest mitochondria was increased (largest mitochondria category, 4: n = 16–17, t_{31} = 2.62, p = 0.013).

(F) 1 h after one-cycle training, no effect was observed on the smallest mitochondria category (1: n = 16, t_{30} = 0.29, p = 0.77), whereas for the other categories, the changes are similar to the ones observed after spaced training (no effect on categories, 2: n = 16, t_{30} = 0.63, p = 0.53 and 3: n = 16, t_{30} = 0.94, p = 0.35; increase for the category, 4: n = 16, t_{30} = 2.47, p = 0.020).

(G) When Miro is knocked down in adult MB, the partial depletion of small mitochondria upon spaced training is no longer observed (smallest mitochondria category, 1: n = 15, t_{28} = 1.27, p = 0.21), whereas for the other mitochondria categories the changes are similar to the ones observed after spaced training in genotypic control flies (no effect on categories, 2: n = 15, t_{28} = 0.25, p = 0.80; 3: n = 15, t_{28} = 0.76, p = 0.45; and increase for the category, 4: n = 15, t_{28} = 2.18, p = 0.038). Bar plots in (E)–(G): mean ± SEM with dots as individual values, unpaired two-tailed t test: * $p < 0.05$, ns, not significant, $p > 0.05$. The indicated "n" is the number of animals that were assayed in each condition. Scale bars: 20 μm in (B), 5 μm in (C), and 2.5 μm in (D)–(G).

See also Videos S1, S2, S3, S4, S5, and S6, Figure S2, and Table S1.

decrease mitochondria density in the soma regardless of the association between odor and electric shocks. 1 h after single-cycle training, small mitochondria density in flies subjected to associative training was similar to experimental control flies (Figure 2F; Video S5). By contrast, the effect of associative single-cycle training on the density of the other categories of mitochondria was the same as of spaced training (Figures 2F and S2F). Altogether, these results show that the partial depletion of small mitochondria from MB neuronal soma occurs specifically upon LTM formation. By contrast, the density of the largest mitochondria increased after both protocols. This suggests that fusion events in the soma could occur for aversive memory formation in general. To test this, we targeted OPA1, which mediates the fusion of mitochondria internal membrane.[60] OPA1 KD in adult MB neurons impaired 24-h memory after spaced training as well as 3-h memory after one-cycle training, whereas memory was normal when RNAi was not induced (Figures S2H–S2K). Thus, although fusion events likely occur in the soma of MB neurons upon aversive associative training, they are not specifically required for LTM formation.

The observed reduction in the density of small mitochondria in MB neuronal soma after spaced training can result from three different phenomena, which are not mutually exclusive: mitophagy, mitochondria fusion events, and/or mitochondria transport out of MB neuronal soma to the axons (Figure S2G). Pink1 and Parkin are two well-known actors of mitophagy,[60] but KD of either Pink1[61] or Parkin in adult MB neurons had no effect on LTM (Figures S2L–S2N). These results show that mitophagy is not required for LTM, thus indicating that mitophagy is not responsible for the decreased density of small mitochondria in MB soma that occurs during LTM formation. An alternative explanation could be the occurrence of mitochondria fusion, in which case the decrease in small mitochondria soma content would be linked to the increase in the density of the large ones. Several lines of evidence, however, argue against this scenario. First, our data obtained after single-cycle training (Figure 2F) indicate that mitochondria fusion already occurs, but independently of any reduction in the density of small mitochondria in MB neuronal soma, suggesting that after repeated cycles, the two observed phenomena are independent. Second, if the increased density of large mitochondria was linked to the fusion of the smallest ones, the mitochondria total volume should not be increased upon LTM formation, contrary to what we observed (Figure S2B). Altogether, these results suggest that the partial depletion of small mitochondria from MB neuronal soma, which occurs specifically after spaced training, is likely to be the result of their transport out of MB neuronal soma, and consequently, impairment of mitochondria motility should hamper this effect. Expression of Miro RNAi in adult MB did not globally affect mitochondria volume as compared with genotypic control flies (Figure S2O), suggesting that Miro KD in adult MB does not induce mitochondria clustering in MB neuronal soma. As in control flies (Figure S2A), associative spaced training did not change mitochondria total density in flies expressing Miro RNAi in adult MB (Figure S2P). However, in flies expressing Miro RNAi in adult MB, we failed to observe a decrease in the density of small mitochondria in MB neuronal soma after associative spaced training (Figure 2G; Video S6). By contrast, Miro KD in MB adult neurons did not change the effect of spaced training on the density of the others categories of mitochondria (Figures 2G and S2Q). Altogether, these results show that spaced training elicits a partial depletion of small mitochondria from MB neuronal soma that relies on Miro-dependent mitochondrial dynamics.

Miro-Milton-dependent mitochondrial dynamics in axons is increased upon LTM formation

In order to directly investigate mitochondrial dynamics in the axonal compartment of MB, we performed *in vivo* fluorescence recovery after photobleaching (FRAP) of dsRed addressed to the mitochondria matrix[47] (the same construct as in Figures 2 and S1), an approach previously used to monitor mitochondria motility in cells *in vitro*.[62] Thus, even if MB axons are tightly bundled and the axons are highly enriched in mitochondria, we expect to be able to estimate mitochondrial dynamics without needing to resolve single mitochondria. The dsRed FRAP kinetic was monitored in the tip of the α lobe (a distal end of axons of α/β KCs) in naive flies expressing either a cytosolic dsRed[63] or the mitochondrial dsRed.[47] As for all *in vivo* imaging experiments performed in our laboratory independently of the type of measurement and fluorescent probe,[34,42,64] we used female flies (see STAR Methods for details). The recovery of fluorescence of the free cytosolic dsRed reached a plateau of about 70% of the initial fluorescence, whereas when the dsRed is trapped inside the mitochondria, the fluorescence recovery index was much slower, and 60 min after bleaching, the fluorescence recovery remained low (less than 4% of the initial fluorescence) (Figure 3A). The slow rate of fluorescence recovery of mitochondrial dsRed compared with free cytosolic dsRed is consistent with previous *in vitro* studies[62] and the high density of mitochondria observed in the axonal compartment of MB, which may limit movement (Figure 2B). We then investigated mitochondria FRAP in the MB axonal compartment upon LTM formation. When flies expressing the mitochondrial dsRed in adult MB were subjected to spaced associative training, the slope of the fluorescence recovery index in the tip of the α lobe was increased compared with experimental control flies (Figure 3B). In flies expressing the mitochondrial dsRed together with Miro RNAi in adult MB, spaced associative training failed to increase mitochondria FRAP in the tip of the α lobe compared with experimental control flies (Figure 3C). We replicated these results in a Milton KD condition (Figure S3). Altogether, these results uncover increased mitochondrial dynamics in the α lobe of MB dependent on Miro-Milton complex upon LTM formation. Together with the Miro-dependent partial depletion of small mitochondria of MB soma occurring specifically upon LTM formation (Figure 2), these results suggest that small mitochondria might be transported along the microtubules from the soma toward the axonal compartment via the Milton-Miro complex.

Miro and Milton are required for axonal upregulation of mitochondrial metabolism upon LTM formation

We next sought to determine why acute activation of mitochondrial dynamics is critical for LTM formation after spaced training. Our previous work showed that single-cycle and spaced training induce distinct spatiotemporal patterns of mitochondrial metabolic activation within MB neurons. Following single-cycle training, increased pyruvate consumption by mitochondria was reported across multiple sites of MB neurons, i.e., both in the

CellPress
OPEN ACCESS

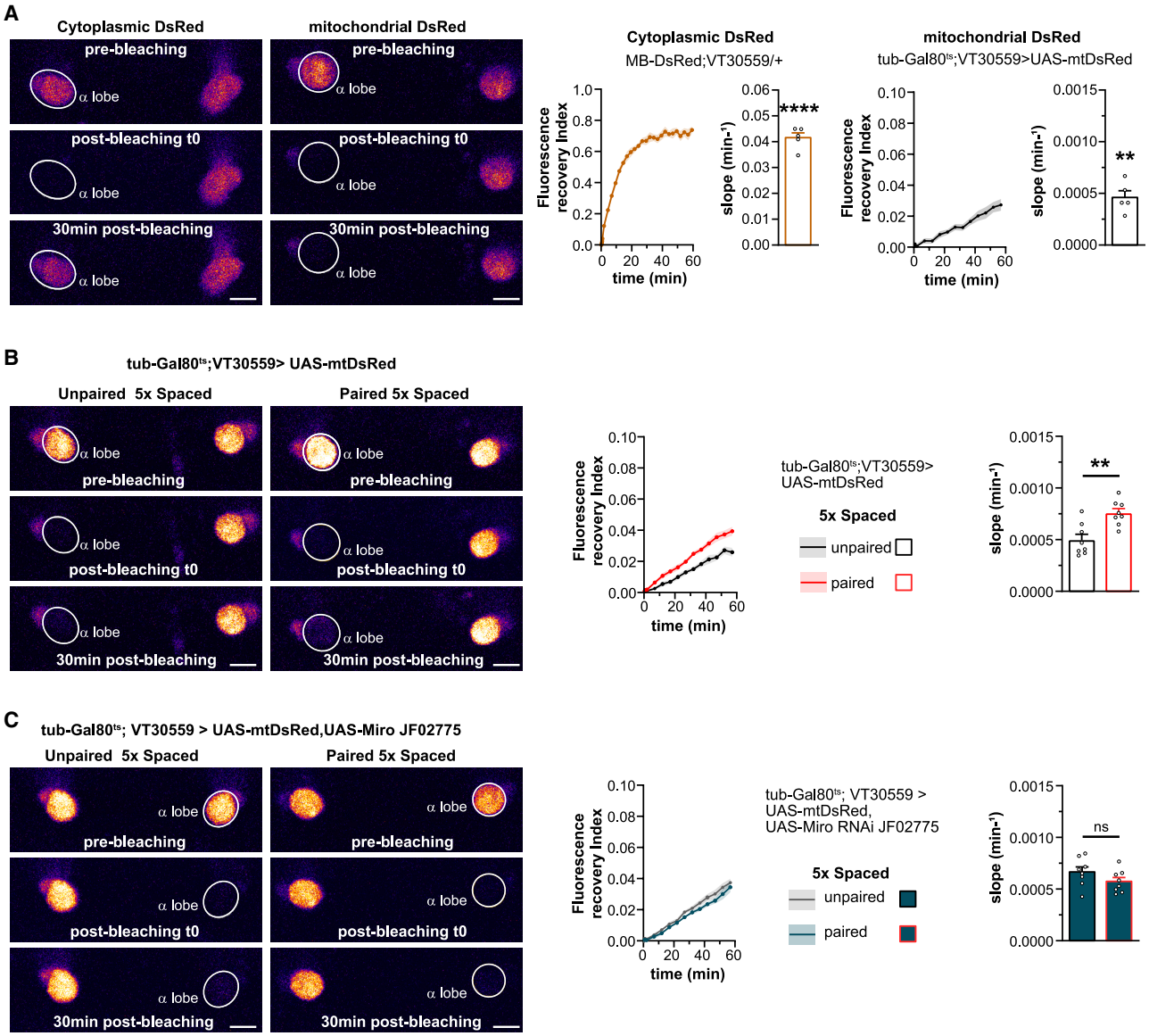

Figure 3. Miro-dependent mitochondrial dynamics in axon are increased upon LTM formation

(A) Representative images of FRAP experiments performed on flies expressing in the MB neurons either cytosolic dsRed (on the left) or mitochondrial dsRed (on the right). A first acquisition (pre-bleaching) was performed before photobleaching one of the α lobes (at the tip, the white circle represents the photobleaching region), while the other lobe was used as a landmark. The acquisition made 10 s post-bleaching allows to control for the efficacy of the bleaching (post-bleaching t0). The 30-min post-bleaching acquisition is shown to illustrate the partial recovery of fluorescence. In flies expressing a cytosolic dsRed in adult MB, the fluorescence recovery index reaches around 70% of the initial fluorescence within 30 min. To quantify the recovery of fluorescence, a slope measurement was made within the time interval when the fluorescence recovery index is linear as a function of time. Thus, for the cytosolic dsRed that can freely diffuse in the cytoplasm, the kinetic of the fluorescence recovery index is relatively fast, and the time window for slope measurement is set to the first 10 min (slope measurement [10 min]: one-sample t test, $n = 5$, $t_4 = 22.2$, $p < 0.0001$). By contrast, for the mt-dsRed, which is spatially constrained into the mitochondria matrix and therefore reflects mitochondria motility, the kinetic of the fluorescence recovery index is slow and does not reach a plateau, so the time window for slope measurement is set to the first 40 min post-bleaching (slope measurement [40 min]: one-sample t test, $n = 5$, $t_4 = 7.06$, $p = 0.002$).

(B) Left: FRAP experiments on flies expressing a mitochondrial dsRed in the adult MB neurons subjected to spaced training (unpaired on the left and paired on the right). Right: kinetic of the fluorescence recovery index: the recovery of mt-dsRed florescence, an index of mitochondria motility, is faster in the α lobe of flies subjected to associative spaced training compared with control flies subjected to non-associative training (unpaired condition) (slope measurement [40 min], $n = 8$ $t_{14} = 3.78$, $p = 0.002$).

(C) Left: FRAP experiments on flies expressing a mitochondrial dsRed together with Miro RNAi in the adult MB neurons subjected to spaced training (unpaired on the left and paired on the right). Right: kinetic of the fluorescence recovery index: Miro KD in adult MB neurons impaired the spaced training-induced increase in the mitochondria motility index (slope measurement [40 min], $n = 8$ $t_{14} = 1.48$, $p = 0.160$). Bar plots: mean ± SEM with dots as individual values; (A) one-sample t test; (B and C) unpaired two-tailed t test. $^{**}p < 0.01$; $^{****}p < 0.0001$ ns, not significant, $p > 0.05$. Scale bars: 20 μm.

See also Figure S3.

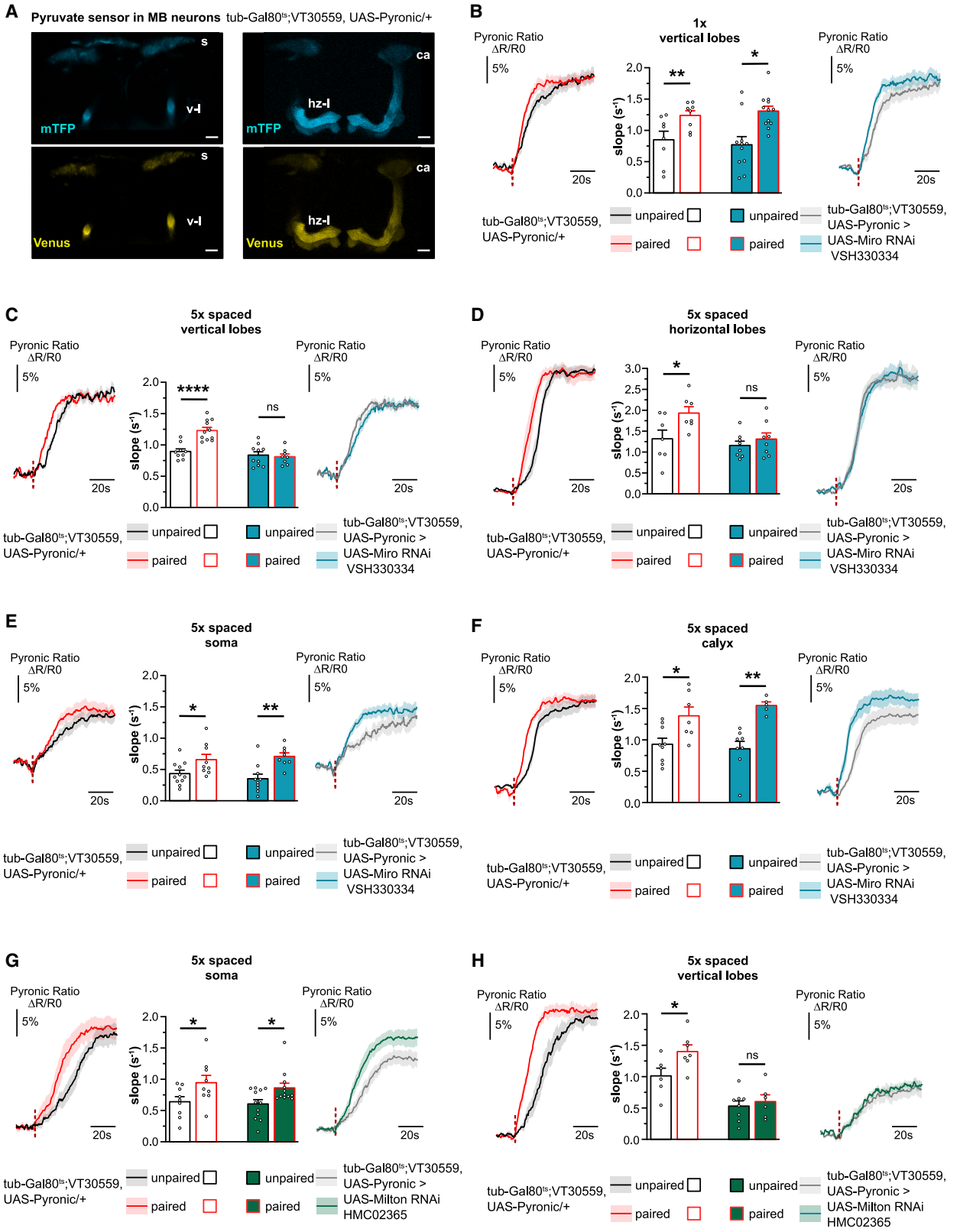

(legend on next page)

CellPress
OPEN ACCESS

soma compartment and in the axonal compartment.[42] After spaced training, a specific dopamine-induced signaling cascade further reinforces this metabolic regulation, specifically at the level of MB axons. This signaling involves activation of the pyruvate dehydrogenase complex and is a limiting step in the initiation of LTM formation.[34] We hypothesized that Miro-Milton-dependent mitochondrial dynamics are specifically required after spaced training for the sustained increase in pyruvate consumption in the axonal compartment. We thus investigated which (if any) of these mitochondrial metabolic changes are sensitive to alterations in mitochondrial dynamics. We used *in vivo* pyruvate imaging experiments to monitor the pyruvate consumption by mitochondria in MB neurons within 1.5 h after training, as previously carried out.[34,42] Briefly, we expressed the pyruvate fluorescence resonance energy transfer (FRET) sensor Pyronic in MB neurons (Figure 4A), and pyruvate flux to the mitochondria was measured using the slope of pyruvate accumulation in the cytosol following the interruption of mitochondrial respiration by application of sodium azide, a blocker of mitochondrial complex IV[34] (see STAR Methods for details). In MB vertical lobes, we observed after one-cycle training an increase in pyruvate flux to the mitochondria of flies trained with paired training in comparison with flies subjected to non-associative training (Figure 4B), as expected from our previous report,[42] and it was insensitive to Miro KD (Figure 4B). Notably, the slope of pyruvate accumulation in the unpaired group was similar between flies expressing or not Miro RNAi in adult MB. Thus, despite 3 days of RNAi induction in which axonal mitochondrial transport has been impaired, mitochondria that are still present in the MB axonal compartment (as seen in Figure S1K) are functional since their ability to metabolize pyruvate is preserved.

We then investigated mitochondria pyruvate consumption after spaced training in the axonal, calyx, and soma compartments. As previously shown,[34] mitochondrial pyruvate flux in the vertical lobes was increased in flies trained with spaced associative training as compared with unpaired flies (Figure 4C). A similar effect was also observed in the horizontal lobes, the other axonal compartment of MB neurons (Figure 4D), as well as in the soma and the dendritic (i.e., calyx) compartments of MB neurons (Figures 4E and 4F, respectively). However, when Miro was knocked down in adult MB neurons, spaced training failed to elicit a higher pyruvate flux in MB axonal compartments (Figures 4C and 4D), whereas it was still observed in the other non-axonal compartments (Figures 4E and 4F). We obtained similar compartmentalized effects in a Milton KD condition (Figures 4G and 4H). Combined, these results show that Miro-Milton-mediated mitochondrial dynamics specifically sustain the increase in mitochondrial pyruvate flux in the MB lobes after spaced training likely by increasing mitochondria number via mitochondria transport. As the occurrence of this axonal upregulation of pyruvate flux to the mitochondria gates LTM formation,[34] our findings altogether reveal a critical role of mitochondrial dynamics in the initiation of LTM consolidation.

DISCUSSION

In this study, we showed *in vivo* that in adult MB neurons, Milton-Miro-dependent mitochondrial dynamics are required for LTM but not for shorter-lasting associative memory. Super-resolution microscopy allowed us to observe that specifically upon LTM formation, a Miro-dependent partial depletion of small mitochondria from the soma occurs, suggesting that the anterograde Miro-mediated transport of mitochondria rather than their retrograde transport is crucial for supporting LTM formation. Using *in vivo* FRAP experiments in MB neurons, we observed that spaced training triggers an increase in axonal mitochondria motility, and this effect requires Miro and Milton. Furthermore, using *in vivo* pyruvate imaging in the axonal, soma, and calyx compartments of MB neurons, we revealed that only upon LTM formation, the upregulation of mitochondrial metabolism is dependent on Milton/Miro-based mitochondria dynamics, specifically in the axonal compartment. Altogether, our data show that to sustain LTM formation, activation of mitochondrial dynamics and transport is critical to satisfy the specific demands of the axonal compartment linked to mitochondria functions, such as energy need.

Memories formed after spaced training or single-cycle training (i.e., LTM and 3-h memory, respectively) both rely on pyruvate mitochondrial oxidation.[34,42] How can we therefore explain the differential dependency on mitochondrial axonal transport between these two types of aversive memories? The upregulation of mitochondrial pyruvate metabolism in response to increased energy demand can be achieved by two non-exclusive,

Figure 4. Miro and Milton are required for axonal upregulation of mitochondrial metabolism upon LTM formation

(A) The pyruvate sensor Pyronic was expressed in adult MB neurons and visualized in the mTFP and Venus channels. The pyruvate FRET signal was quantified in the different cellular compartments of MB neurons: the axonal compartments: the vertical lobes (v-l); the horizontal lobes (h-l); the soma (s); and the calyx (Ca). Scale bars: 20 μm.

(B) One-cycle training elicited a faster pyruvate accumulation in MB neuron axons after sodium azide application compared with non-associative unpaired training (left: $n = 11–12$, $t_{21} = 3.64$, $p = 0.0015$). When Miro was knocked down in adult MB neurons, this effect was preserved (right: $n = 8$, $t_{14} = 2.50$, $p = 0.026$).

(C and D) Spaced training elicited a faster pyruvate accumulation in the axonal compartment, both in the vertical and the horizontal lobes after sodium azide application (C, vertical lobes, left: $n = 9–11$, $t_{18} = 5.07$, $p < 0.0001$; D, horizontal lobes, left: $n = 7$, $t_{12} = 2.39$, $p = 0.034$). This effect was impaired in both axonal compartments by Miro KD in adult MB neurons (C, vertical lobes, right: $n = 8–10$, $t_{16} = 0.33$, $p = 0.74$; D, horizontal lobes, right: $n = 8$, $t_{14} = 0.8511$, $p = 0.409$).

(E and F) The increased mitochondrial pyruvate flux elicited by spaced training in either the soma (E, $n = 9–11$, $t_{18} = 2.27$, $p = 0.036$) or the calyx (F, $n = 7–9$, $t_{14} = 2.75$, $p = 0.016$) was not affected by Miro KD in adult MB neurons (E: soma $n = 8–10$, $t_{16} = 3.70$, $p = 0.002$, F: calyx $n = 5–8$, $t_{11} = 4.32$, $p = 0.001$).

(G and H) The increased mitochondrial pyruvate flux elicited by spaced training in the soma (G, $n = 9$, $t_{16} = 2.13$, $p = 0.048$) was not affected by Milton KD in adult MB neurons (G, $n = 12$, $t_{22} = 2.53$, $p = 0.019$), whereas in the axonal comportment (H, $n = 6–7$, $t_{11} = 2.40$, $p = 0.035$), this effect was impaired by Milton KD (H, $n = 6–8$, $t_{12} = 0.53$, $p = 0.606$). It should be noted that the reduced pyruvate flux to the mitochondria in the unpaired Milton KD flies compared with unpaired genotypic controls is likely due to the strong decrease in mitochondria axonal content in these flies (Figure S1C), whereas in the soma where mitochondria content is not decreased, the pyruvate flux to the mitochondria is similar to the genotypic controls. Bar plots: mean ± SEM with dots as individual values, unpaired two-tailed t test. $^{*}p < 0.05$; $^{**}p < 0.01$; $^{****}p < 0.0001$, ns, not significant, $p > 0.05$. (B–H) Dashed red line: time of sodium azide application (5 mM).

alternative mechanisms: the local increase in mitochondria number and the upregulation of the Krebs cycle and respiratory chain activities via a signaling pathway activated upon neuronal activation, such as the local increase in Ca^{2+} as revealed *in vitro* in hippocampal neurons.[65–67] Our results show that the upregulation of mitochondrial metabolism elicited by single-cycle training is not dependent on Miro-based mitochondrial dynamics, suggesting that increasing the rate of oxidative phosphorylation via enzymatic regulation is sufficient to upregulate pyruvate flux to sustain 3-h memory formation. However, to sustain LTM formation, the arrival of additional mitochondria in the axonal compartment is critical to mediate the upregulation of mitochondrial metabolism. Whereas we previously monitored this metabolism upregulation in only one of the axonal compartments,[34] the vertical lobes, here we revealed that it also occurs in the medial lobes and that in both axonal compartments it is dependent on mitochondria axonal trafficking. Intriguingly, a two-component model for LTM was recently proposed in which the efferent pathways include output from both vertical and medial lobes,[41] and whether such a model is consistent with our finding would need further investigation. We can also speculate about the time limits of this process. The duration of this increase in mitochondria trafficking was not addressed in this study. However, we recently demonstrated that after spaced training, the upregulation of mitochondria pyruvate metabolism lasts for at least 6 h post-training in the vertical lobe, whereas upon single-cycle training, it lasts less than 2 h post-training.[68] Thus, it is possible that the mitochondria transport to the axonal compartment that we reveal here as critical to LTM formation is increased for several hours after training. Altogether, the data suggest that the long-lasting increased demand in energy and/or byproducts of pyruvate mitochondrial metabolism cannot be fulfilled by enzymatic upregulation of mitochondria respiratory capacity alone, but that it requires a specific mechanism to trigger mitochondrial trafficking toward the axons.

A limitation of our study is that all of the changes triggered by spaced training are observed at the MB neuronal population level, whereas the odors used in the classical olfactory memory paradigm activate a sparse population of MB neurons, and the associative memory is encoded only in a small subset of neurons.[69,70] Currently, we cannot exclude either of the following two possibilities: (1) that the observed changes are restricted to odor-responsive cells; and (2) that learning, and in particular LTM formation, induces a global metabolic shift in all (or a large part of) KC independently of their odor responsiveness.

Our data reveal that mitochondria functions are regulated in a compartment-specific manner, both at the basal state and upon memory formation. At the basal state, we observed that *in vivo* pyruvate mitochondrial consumption is lower in the soma as compared with the axons and the calyx (Figure 4, see flies subjected to a non-associative protocol, i.e., unpaired spaced training), possibly due to less oxidative phosphorylation activity and/or fewer mitochondria. This second alternative is supported both by the literature on mammalian neurons[8,57,58] and by our observation in *Drosophila* using classical confocal microscopy, showing a higher density of mitochondria in the lobes and the calyx area as compared with the soma region (Figure 2B). Biochemical studies on synaptic and "non-synaptic" mitochondria,[71] as well as more recent proteomics studies,[72] in both cases on mammalian neurons, suggest that heterogeneity in mitochondrial metabolism across compartments may also exist. In addition to this specific metabolic signature of somatic mitochondria at the basal state, we found in MB soma that both single-cycle and spaced associative training elicit changes in mitochondria at the morphological level with an increase in density of the largest mitochondria (Figure 2) and at the functional level with an increase in pyruvate mitochondrial consumption independent of the Miro-Milton complex (Rabah et al.[42]; Figures 4E and 4G). This suggests that this local metabolic regulation relies on the accumulation of larger mitochondria in the same compartment, as it is also the case in the calyx. Thus, Miro/Milton involvement allows separating, at the mechanistic level, metabolic regulations triggered by spaced training occurring in the soma and the calyx from those occurring in the axons.

Pioneering genetic studies in *Drosophila* were essential in identifying the Miro/Milton complex and its function in mitochondria transport in axons.[23,25,26] However, most of these studies were conducted in larvae and at the neuromuscular junction, due to the lethality of the Milton and Miro mutants. Whereas global deletion of Miro1 in mammals is perinatally lethal,[19] the conditional loss of Miro1, depending on the neuronal type, results in partial depletion of mitochondria either in axons or in the dendritic arborization, with functional consequences ranging from altered network activity and reduction of anxiety-like behavior to dendritic degeneration and cell death.[20,21] Here, we use an RNAi strategy to downregulate Miro or Milton in adult MB neurons to avoid drastic depletion of mitochondria axonal content leading to neurodegeneration. As KDs induced by RNAi are always partial and the strength of one specific RNAi cannot be predicted, differences in axonal basal distribution of mitochondrial were observed between RNAi lines targeting Miro or Milton. They were detectable both at the anatomical level (Figures S1 and S3) and the functional level (basal mitochondria pyruvate flux in Figure 4). However, regardless of the RNAi line used to downregulate Miro or Milton in adult MB, we observed that the Miro-Milton complex is required specifically for establishing associative LTM. Importantly, our data point to the transport of mitochondria to the axonal compartment as being the primary cause of LTM impairment, showing that the memory defect is not related to neurodegeneration caused by accumulation of damaged mitochondria in the axonal terminal. Therefore, our work establishes that altering the machinery of mitochondria axonal transport results in memory impairment, independently of the neurodegeneration phenomena described using a cell-specific loss-of-function model. Although an increasing number of studies suggest that mitochondria trafficking in neurons is impaired in neurodegenerative diseases such as Alzheimer's disease,[73,74] our work provides a framework to understand the link between mitochondria transport and the early symptoms of memory impairment in neurodegenerative diseases.

STAR★METHODS

Detailed methods are provided in the online version of this paper and include the following:

- KEY RESOURCES TABLE
- RESOURCE AVAILABILITY

- Lead contact
- Materials availability
- Data and code availability
- EXPERIMENTAL MODEL AND SUBJECT DETAILS
- METHOD DETAILS
  - Olfactory conditioning and memory test
  - Confocal imaging of mitochondria in naive flies
  - Immunostaining for STED microscopy
  - Image acquisition and analysis of immunostaining
  - *In vivo* imaging
  - qPCR validation of RNAi lines
- QUANTIFICATION AND STATISTICAL ANALYSIS

SUPPLEMENTAL INFORMATION

Supplemental information can be found online at https://doi.org/10.1016/j.cub.2024.03.050.

ACKNOWLEDGMENTS

We thank the TriP consortium at Harvard Medical School (NIH/NIGMS R01-GM084947) for providing transgenic RNAi fly stocks. We thank Alexandre Didelet and Christelle Beauchamp for technical support with fly food preparation, Milena Usi for assistance with behavioral experiments, and Olivier Renaud for advice about FRAP experiments. The authors acknowledge funding from the European Research Council (ERC Advanced Grant EnergyMemo no. 741550, to T.P.) and from the Agence Nationale de la Recherche (ANR Metabolic Brain Aging no. 20-CE92-0047-01 to P.-Y.P.). T.C. was funded for 3 years by a doctoral fellowship from the French Ministry of Research, and for her fourth doctoral year, she was funded by the Fondation pour la Recherche Medicale (FRM), grant number FDT202304016704.

AUTHOR CONTRIBUTIONS

Conceptualization: A.P., P.-Y.P., and T.P.; methodology: A.P., P.-Y.P., L.D., and P.B.; investigation: A.P., J.M., T.C., and D.G.; supervision: A.P., P.-Y.P., and T.P.; writing – original draft: A.P.; writing – review and editing: A.P., P.-Y.P., and T.P.; funding acquisition: T.P. and P.-Y.P.

DECLARATION OF INTERESTS

The authors declare no competing interests.

Received: January 23, 2023
Revised: December 21, 2023
Accepted: March 25, 2024
Published: April 19, 2024

REFERENCES

1. Hall, C.N., Klein-Flügge, M.C., Howarth, C., and Attwell, D. (2012). Oxidative Phosphorylation, Not Glycolysis, Powers Presynaptic and Postsynaptic Mechanisms Underlying Brain Information Processing. J. Neurosci. *32*, 8940–8951. https://doi.org/10.1523/JNEUROSCI.0026-12.2012.
2. Brini, M., Calì, T., Ottolini, D., and Carafoli, E. (2014). Neuronal calcium signaling: function and dysfunction. Cell. Mol. Life Sci. *71*, 2787–2814. https://doi.org/10.1007/s00018-013-1550-7.
3. Accardi, M.V., Daniels, B.A., Brown, P.M.G.E., Fritschy, J.-M., Tyagarajan, S.K., and Bowie, D. (2014). Mitochondrial reactive oxygen species regulate the strength of inhibitory GABA-mediated synaptic transmission. Nat. Commun. *5*, 3168. https://doi.org/10.1038/ncomms4168.
4. Szutowicz, A., Bielarczyk, H., Jankowska-Kulawy, A., Pawełczyk, T., and Ronowska, A. (2013). Acetyl-CoA the Key Factor for Survival or Death of Cholinergic Neurons in Course of Neurodegenerative Diseases. Neurochem. Res. *38*, 1523–1542. https://doi.org/10.1007/s11064-013-1060-x.
5. Kann, O., and Kovács, R. (2007). Mitochondria and neuronal activity. Am. J. Physiol. Cell Physiol. *292*, C641–C657. https://doi.org/10.1152/ajpcell.00222.2006.
6. Rowley, N.M., Madsen, K.K., Schousboe, A., and Steve White, H. (2012). Glutamate and GABA synthesis, release, transport and metabolism as targets for seizure control. Neurochem. Int. *61*, 546–558. https://doi.org/10.1016/j.neuint.2012.02.013.
7. Kuznetsov, A.V., Hermann, M., Saks, V., Hengster, P., and Margreiter, R. (2009). The cell-type specificity of mitochondrial dynamics. Int. J. Biochem. Cell Biol. *41*, 1928–1939. https://doi.org/10.1016/j.biocel.2009.03.007.
8. Pekkurnaz, G., and Wang, X. (2022). Mitochondrial heterogeneity and homeostasis through the lens of a neuron. Nat. Metab. *4*, 802–812. https://doi.org/10.1038/s42255-022-00594-w.
9. Harris, J.J., Jolivet, R., and Attwell, D. (2012). Synaptic Energy Use and Supply. Neuron *75*, 762–777. https://doi.org/10.1016/j.neuron.2012.08.019.
10. Saxton, W.M., and Hollenbeck, P.J. (2012). The axonal transport of mitochondria. J. Cell Sci. *125*, 2095–2104. https://doi.org/10.1242/jcs.053850.
11. Sheng, Z.-H. (2017). The Interplay of Axonal Energy Homeostasis and Mitochondrial Trafficking and Anchoring. Trends Cell Biol. *27*, 403–416. https://doi.org/10.1016/j.tcb.2017.01.005.
12. Li, Z., Okamoto, K.-I., Hayashi, Y., and Sheng, M. (2004). The Importance of Dendritic Mitochondria in the Morphogenesis and Plasticity of Spines and Synapses. Cell *119*, 873–887. https://doi.org/10.1016/j.cell.2004.11.003.
13. Chang, D.T.W., Honick, A.S., and Reynolds, I.J. (2006). Mitochondrial Trafficking to Synapses in Cultured Primary Cortical Neurons. J. Neurosci. *26*, 7035–7045. https://doi.org/10.1523/JNEUROSCI.1012-06.2006.
14. Su, B., Ji, Y.-S., Sun, X.L., Liu, X.-H., and Chen, Z.-Y. (2014). Brain-derived Neurotrophic Factor (BDNF)-induced Mitochondrial Motility Arrest and Presynaptic Docking Contribute to BDNF-enhanced Synaptic Transmission. J. Biol. Chem. *289*, 1213–1226. https://doi.org/10.1074/jbc.M113.526129.
15. Li, S., Xiong, G.-J., Huang, N., and Sheng, Z.-H. (2020). The cross-talk of energy sensing and mitochondrial anchoring sustains synaptic efficacy by maintaining presynaptic metabolism. Nat. Metab. *2*, 1077–1095. https://doi.org/10.1038/s42255-020-00289-0.
16. Divakaruni, S.S., Van Dyke, A.M., Chandra, R., LeGates, T.A., Contreras, M., Dharmasri, P.A., Higgs, H.N., Lobo, M.K., Thompson, S.M., and Blanpied, T.A. (2018). Long-Term Potentiation Requires a Rapid Burst of Dendritic Mitochondrial Fission during Induction. Neuron *100*, 860–875.e7. https://doi.org/10.1016/j.neuron.2018.09.025.
17. Verstreken, P., Ly, C.V., Venken, K.J.T., Koh, T.-W., Zhou, Y., and Bellen, H.J. (2005). Synaptic Mitochondria Are Critical for Mobilization of Reserve Pool Vesicles at Drosophila Neuromuscular Junctions. Neuron *47*, 365–378. https://doi.org/10.1016/j.neuron.2005.06.018.
18. Barel, O., Malicdan, M.C.V., Ben-Zeev, B., Kandel, J., Pri-Chen, H., Stephen, J., Castro, I.G., Metz, J., Atawa, O., Moshkovitz, S., et al. (2017). Deleterious variants in TRAK1 disrupt mitochondrial movement and cause fatal encephalopathy. Brain *140*, 568–581. https://doi.org/10.1093/brain/awx002.
19. Nguyen, T.T., Oh, S.S., Weaver, D., Lewandowska, A., Maxfield, D., Schuler, M.-H., Smith, N.K., Macfarlane, J., Saunders, G., Palmer, C.A., et al. (2014). Loss of Miro1-directed mitochondrial movement results in a novel murine model for neuron disease. Proc. Natl. Acad. Sci. USA *111*, E3631–E3640. https://doi.org/10.1073/pnas.1402449111.
20. Kontou, G., Antonoudiou, P., Podpolny, M., Szulc, B.R., Arancibia-Carcamo, I.L., Higgs, N.F., Lopez-Domenech, G., Salinas, P.C., Mann, E.O., and Kittler, J.T. (2021). Miro1-dependent mitochondrial dynamics in parvalbumin interneurons. eLife *10*, e65215. https://doi.org/10.7554/eLife.65215.

21. López-Doménech, G., Higgs, N.F., Vaccaro, V., Roš, H., Arancibia-Cárcamo, I.L., MacAskill, A.F., and Kittler, J.T. (2016). Loss of Dendritic Complexity Precedes Neurodegeneration in a Mouse Model with Disrupted Mitochondrial Distribution in Mature Dendrites. Cell Rep. *17*, 317–327. https://doi.org/10.1016/j.celrep.2016.09.004.

22. Sheng, Z.-H., and Cai, Q. (2012). Mitochondrial transport in neurons: impact on synaptic homeostasis and neurodegeneration. Nat. Rev. Neurosci. *13*, 77–93. https://doi.org/10.1038/nrn3156.

23. Stowers, R.S., Megeath, L.J., Górska-Andrzejak, J., Meinertzhagen, I.A., and Schwarz, T.L. (2002). Axonal Transport of Mitochondria to Synapses Depends on Milton, a Novel Drosophila Protein. Neuron *36*, 1063–1077. https://doi.org/10.1016/S0896-6273(02)01094-2.

24. Glater, E.E., Megeath, L.J., Stowers, R.S., and Schwarz, T.L. (2006). Axonal transport of mitochondria requires milton to recruit kinesin heavy chain and is light chain independent. J. Cell Biol. *173*, 545–557. https://doi.org/10.1083/jcb.200601067.

25. Guo, X., Macleod, G.T., Wellington, A., Hu, F., Panchumarthi, S., Schoenfield, M., Marin, L., Charlton, M.P., Atwood, H.L., and Zinsmaier, K.E. (2005). The GTPase dMiro Is Required for Axonal Transport of Mitochondria to Drosophila Synapses. Neuron *47*, 379–393. https://doi.org/10.1016/j.neuron.2005.06.027.

26. Pilling, A.D., Horiuchi, D., Lively, C.M., and Saxton, W.M. (2006). Kinesin-1 and Dynein Are the Primary Motors for Fast Transport of Mitochondria in Drosophila Motor Axons. Mol. Biol. Cell *17*, 2057–2068. https://doi.org/10.1091/mbc.e05-06-0526.

27. Tanaka, Y., Kanai, Y., Okada, Y., Nonaka, S., Takeda, S., Harada, A., and Hirokawa, N. (1998). Targeted Disruption of Mouse Conventional Kinesin Heavy Chain kif5B, Results in Abnormal Perinuclear Clustering of Mitochondria. Cell *93*, 1147–1158. https://doi.org/10.1016/S0092-8674(00)81459-2.

28. Hurd, D.D., and Saxton, W.M. (1996). Kinesin Mutations Cause Motor Neuron Disease Phenotypes by Disrupting Fast Axonal Transport in Drosophila. Genetics *144*, 1075–1085. https://doi.org/10.1093/genetics/144.3.1075.

29. Schwarz, T.L. (2013). Mitochondrial Trafficking in Neurons. Cold Spring Harb. Perspect. Biol. *5*, a011304. https://doi.org/10.1101/cshperspect.a011304.

30. Fenton, A.R., Jongens, T.A., and Holzbaur, E.L.F. (2021). Mitochondrial adaptor TRAK2 activates and functionally links opposing kinesin and dynein motors. Nat. Commun. *12*, 4578. https://doi.org/10.1038/s41467-021-24862-7.

31. Aso, Y., Hattori, D., Yu, Y., Johnston, R.M., Iyer, N.A., Ngo, T.-T.B., Dionne, H., Abbott, L.F., Axel, R., Tanimoto, H., et al. (2014). The neuronal architecture of the mushroom body provides a logic for associative learning. eLife *3*, e04577. https://doi.org/10.7554/eLife.04577.

32. Bouzaiane, E., Trannoy, S., Scheunemann, L., Plaçais, P.-Y., and Preat, T. (2015). Two Independent Mushroom Body Output Circuits Retrieve the Six Discrete Components of Drosophila Aversive Memory. Cell Rep. *11*, 1280–1292. https://doi.org/10.1016/j.celrep.2015.04.044.

33. Quinn, W.G., Harris, W.A., and Benzer, S. (1974). Conditioned Behavior in Drosophila melanogaster. Proc. Natl. Acad. Sci. USA *71*, 708–712. https://doi.org/10.1073/pnas.71.3.708.

34. Plaçais, P.-Y., de Tredern, É., Scheunemann, L., Trannoy, S., Goguel, V., Han, K.-A., Isabel, G., and Preat, T. (2017). Upregulated energy metabolism in the Drosophila mushroom body is the trigger for long-term memory. Nat. Commun. *8*, 15510. https://doi.org/10.1038/ncomms15510.

35. Yu, D., Akalal, D.-B.G., and Davis, R.L. (2006). Drosophila alpha/beta mushroom body neurons form a branch-specific, long-term cellular memory trace after spaced olfactory conditioning. Neuron *52*, 845–855. https://doi.org/10.1016/j.neuron.2006.10.030.

36. Heisenberg, M. (2003). Mushroom body memoir: from maps to models. Nat. Rev. Neurosci. *4*, 266–275. https://doi.org/10.1038/nrn1074.

37. Lin, A.C., Bygrave, A.M., de Calignon, A., Lee, T., and Miesenböck, G. (2014). Sparse, decorrelated odor coding in the mushroom body enhances learned odor discrimination. Nat. Neurosci. *17*, 559–568. https://doi.org/10.1038/nn.3660.

38. Tully, T., Preat, T., Boynton, S.C., and Del Vecchio, M. (1994). Genetic dissection of consolidated memory in Drosophila. Cell *79*, 35–47. https://doi.org/10.1016/0092-8674(94)90398-0.

39. Tully, T., and Quinn, W.G. (1985). Classical conditioning and retention in normal and mutant Drosophila melanogaster. J. Comp. Physiol. A *157*, 263–277. https://doi.org/10.1007/BF01350033.

40. Yin, J.C.P., Wallach, J.S., Del Vecchio, M., Wilder, E.L., Zhou, H., Quinn, W.G., and Tully, T. (1994). Induction of a dominant negative CREB transgene specifically blocks long-term memory in Drosophila. Cell *79*, 49–58. https://doi.org/10.1016/0092-8674(94)90399-9.

41. Jacob, P.F., and Waddell, S. (2020). Spaced Training Forms Complementary Long-Term Memories of Opposite Valence in Drosophila. Neuron *106*, 977–991.e4. https://doi.org/10.1016/j.neuron.2020.03.013.

42. Rabah, Y., Francés, R., Minatchy, J., Guédon, L., Desnous, C., Plaçais, P.-Y., and Preat, T. (2023). Glycolysis-derived alanine from glia fuels neuronal mitochondria for memory in Drosophila. Nat. Metab. *5*, 2002–2019. https://doi.org/10.1038/s42255-023-00910-y.

43. McGuire, S.E., Le, P.T., Osborn, A.J., Matsumoto, K., and Davis, R.L. (2003). Spatiotemporal Rescue of Memory Dysfunction in Drosophila. Science *302*, 1765–1768. https://doi.org/10.1126/science.1089035.

44. Iijima-Ando, K., Sekiya, M., Maruko-Otake, A., Ohtake, Y., Suzuki, E., Lu, B., and Iijima, K.M. (2012). Loss of Axonal Mitochondria Promotes Tau-Mediated Neurodegeneration and Alzheimer's Disease–Related Tau Phosphorylation Via PAR-1. PLoS Genet. *8*, e1002918. https://doi.org/10.1371/journal.pgen.1002918.

45. Liu, S., Sawada, T., Lee, S., Yu, W., Silverio, G., Alapatt, P., Millan, I., Shen, A., Saxton, W., Kanao, T., et al. (2012). Parkinson's Disease–Associated Kinase PINK1 Regulates Miro Protein Level and Axonal Transport of Mitochondria. PLoS Genet. *8*, e1002537. https://doi.org/10.1371/journal.pgen.1002537.

46. Vagnoni, A., Hoffmann, P.C., and Bullock, S.L. (2016). Reducing Lissencephaly-1 levels augments mitochondrial transport and has a protective effect in adult Drosophila neurons. J. Cell Sci. *129*, 178–190. https://doi.org/10.1242/jcs.179184.

47. Lutas, A., Wahlmark, C.J., Acharjee, S., and Kawasaki, F. (2012). Genetic Analysis in Drosophila Reveals a Role for the Mitochondrial Protein P32 in Synaptic Transmission. G3 (Bethesda) *2*, 59–69. https://doi.org/10.1534/g3.111.001586.

48. Pascual, A., and Préat, T. (2001). Localization of long-term memory within the Drosophila mushroom body. Science *294*, 1115–1117. https://doi.org/10.1126/science.1064200.

49. Séjourné, J., Plaçais, P.-Y., Aso, Y., Siwanowicz, I., Trannoy, S., Thoma, V., Tedjakumala, S.R., Rubin, G.M., Tchénio, P., Ito, K., et al. (2011). Mushroom body efferent neurons responsible for aversive olfactory memory retrieval in Drosophila. Nat. Neurosci. *14*, 903–910. https://doi.org/10.1038/nn.2846.

50. Bossing, T., Barros, C.S., Fischer, B., Russell, S., and Shepherd, D. (2012). Disruption of Microtubule Integrity Initiates Mitosis during CNS Repair. Dev. Cell *23*, 433–440. https://doi.org/10.1016/j.devcel.2012.06.002.

51. Saotome, M., Safiulina, D., Szabadkai, G., Das, S., Fransson, A., Aspenstrom, P., Rizzuto, R., and Hajnóczky, G. (2008). Bidirectional Ca2+-dependent control of mitochondrial dynamics by the Miro GTPase. Proc. Natl. Acad. Sci. USA *105*, 20728–20733. https://doi.org/10.1073/pnas.0808953105.

52. Ding, L., Lei, Y., Han, Y., Li, Y., Ji, X., and Liu, L. (2016). Vimar Is a Novel Regulator of Mitochondrial Fission through Miro. PLoS Genet. *12*, e1006359. https://doi.org/10.1371/journal.pgen.1006359.

53. Messina, F., Cecconi, F., and Rodolfo, C. (2020). Do You Remember Mitochondria? Front. Physiol. *11*, 271. https://doi.org/10.3389/fphys.2020.00271.

54. Russo, G.J., Louie, K., Wellington, A., Macleod, G.T., Hu, F., Panchumarthi, S., and Zinsmaier, K.E. (2009). Drosophila Miro Is Required for Both

Anterograde and Retrograde Axonal Mitochondrial Transport. J. Neurosci. *29*, 5443–5455. https://doi.org/10.1523/JNEUROSCI.5417-08.2009.

55. Tsai, P.-I., Papakyrikos, A.M., Hsieh, C.-H., and Wang, X. (2017). *Drosophila* MIC60/mitofilin conducts dual roles in mitochondrial motility and crista structure. Mol. Biol. Cell *28*, 3471–3479. https://doi.org/10.1091/mbc.E17-03-0177.
56. Vagnoni, A., and Bullock, S.L. (2018). A cAMP/PKA/Kinesin-1 Axis Promotes the Axonal Transport of Mitochondria in Aging Drosophila Neurons. Curr. Biol. *28*, 1265–1272.e4. https://doi.org/10.1016/j.cub.2018.02.048.
57. Popov, V., Medvedev, N.I., Davies, H.A., and Stewart, M.G. (2005). Mitochondria form a filamentous reticular network in hippocampal dendrites but are present as discrete bodies in axons: A three-dimensional ultrastructural study. J. Comp. Neurol. *492*, 50–65. https://doi.org/10.1002/cne.20682.
58. Faitg, J., Lacefield, C., Davey, T., White, K., Laws, R., Kosmidis, S., Reeve, A.K., Kandel, E.R., Vincent, A.E., and Picard, M. (2021). 3D neuronal mitochondrial morphology in axons, dendrites, and somata of the aging mouse hippocampus. Cell Rep. *36*, 109509. https://doi.org/10.1016/j.celrep.2021.109509.
59. Bun, P. (2022). Minimal Enveloppe Estimation. Version 0.8 (Zenodo). https://doi.org/10.5281/ZENODO.7118602.
60. El-Hattab, A.W., Suleiman, J., Almannai, M., and Scaglia, F. (2018). Mitochondrial dynamics: Biological roles, molecular machinery, and related diseases. Mol. Genet. Metab. *125*, 315–321. https://doi.org/10.1016/j.ymgme.2018.10.003.
61. Sun, X., Duan, Y., Qin, C., Li, J.-C., Duan, G., Deng, X., Ni, J., Cao, X., Xiang, K., Tian, K., et al. (2018). Distinct multilevel misregulations of Parkin and PINK1 revealed in cell and animal models of TDP-43 proteinopathy. Cell Death Dis. *9*, 953. https://doi.org/10.1038/s41419-018-1022-y.
62. Collins, T.J., and Bootman, M.D. (2003). Mitochondria are morphologically heterogeneous within cells. J. Exp. Biol. *206*, 1993–2000. https://doi.org/10.1242/jeb.00244.
63. Riemensperger, T., Völler, T., Stock, P., Buchner, E., and Fiala, A. (2005). Punishment Prediction by Dopaminergic Neurons in Drosophila. Curr. Biol. *15*, 1953–1960. https://doi.org/10.1016/j.cub.2005.09.042.
64. Silva, B., Mantha, O.L., Schor, J., Pascual, A., Plaçais, P.-Y., Pavlowsky, A., and Preat, T. (2022). Glia fuel neurons with locally synthesized ketone bodies to sustain memory under starvation. Nat. Metab. *4*, 213–224. https://doi.org/10.1038/s42255-022-00528-6.
65. de Juan-Sanz, J., Holt, G.T., Schreiter, E.R., de Juan, F., Kim, D.S., and Ryan, T.A. (2017). Axonal Endoplasmic Reticulum Ca2+ Content Controls Release Probability in CNS Nerve Terminals. Neuron *93*, 867–881.e6. https://doi.org/10.1016/j.neuron.2017.01.010.
66. Rangaraju, V., Calloway, N., and Ryan, T.A. (2014). Activity-Driven Local ATP Synthesis Is Required for Synaptic Function. Cell *156*, 825–835. https://doi.org/10.1016/j.cell.2013.12.042.
67. Ashrafi, G., de Juan-Sanz, J., Farrell, R.J., and Ryan, T.A. (2020). Molecular Tuning of the Axonal Mitochondrial Ca2+ Uniporter Ensures Metabolic Flexibility of Neurotransmission. Neuron *105*, 678–687.e5. https://doi.org/10.1016/j.neuron.2019.11.020.
68. Comyn, T., Preat, T., Pavlowsky, A., and Placais, P.-Y. (2023). PKCδ is an activator of neuronal mitochondrial metabolism that mediates the spacing effect on memory consolidation. Preprint at bioRxiv. https://doi.org/10.1101/2023.10.06.561186.
69. Honegger, K.S., Campbell, R.A.A., and Turner, G.C. (2011). Cellular-Resolution Population Imaging Reveals Robust Sparse Coding in the Drosophila Mushroom Body. J. Neurosci. *31*, 11772–11785. https://doi.org/10.1523/JNEUROSCI.1099-11.2011.
70. Hige, T., Aso, Y., Modi, M.N., Rubin, G.M., and Turner, G.C. (2015). Heterosynaptic Plasticity Underlies Aversive Olfactory Learning in Drosophila. Neuron *88*, 985–998. https://doi.org/10.1016/j.neuron.2015.11.003.
71. Lai, J.C.K., Walsh, J.M., Dennis, S.C., and Clark, J.B. (1977). Synaptic and Non-Synaptic Mitochondria from Rat Brain: Isolation and Characterization. J. Neurochem. *28*, 625–631. https://doi.org/10.1111/j.1471-4159.1977.tb10434.x.
72. Graham, L.C., Eaton, S.L., Brunton, P.J., Atrih, A., Smith, C., Lamont, D.J., Gillingwater, T.H., Pennetta, G., Skehel, P., and Wishart, T.M. (2017). Proteomic profiling of neuronal mitochondria reveals modulators of synaptic architecture. Mol. Neurodegener. *12*, 77. https://doi.org/10.1186/s13024-017-0221-9.
73. Panchal, K., and Tiwari, A.K. (2021). Miro (Mitochondrial Rho GTPase), a key player of mitochondrial axonal transport and mitochondrial dynamics in neurodegenerative diseases. Mitochondrion *56*, 118–135. https://doi.org/10.1016/j.mito.2020.10.005.
74. Panchal, K., and Tiwari, A.K. (2020). Miro, a Rho GTPase genetically interacts with Alzheimer's disease-associated genes (Tau, Aβ42 and Appl) in Drosophila melanogaster. Biol. Open *9*, bio049569. https://doi.org/10.1242/bio.049569.
75. Turrel, O., Goguel, V., and Preat, T. (2018). Amnesiac Is Required in the Adult Mushroom Body for Memory Formation. J. Neurosci. *38*, 9202–9214. https://doi.org/10.1523/JNEUROSCI.0876-18.2018.
76. de Chaumont, F., Dallongeville, S., Chenouard, N., Hervé, N., Pop, S., Provoost, T., Meas-Yedid, V., Pankajakshan, P., Lecomte, T., Le Montagner, Y., et al. (2012). Icy: an open bioimage informatics platform for extended reproducible research. Nat. Methods *9*, 690–696. https://doi.org/10.1038/nmeth.2075.
77. Musso, P.-Y., Tchenio, P., and Preat, T. (2015). Delayed Dopamine Signaling of Energy Level Builds Appetitive Long-Term Memory in Drosophila. Cell Rep. *10*, 1023–1031. https://doi.org/10.1016/j.celrep.2015.01.036.
78. Scheunemann, L., Plaçais, P.-Y., Dromard, Y., Schwärzel, M., and Preat, T. (2018). Dunce Phosphodiesterase Acts as a Checkpoint for Drosophila Long-Term Memory in a Pair of Serotonergic Neurons. Neuron *98*, 350–365.e5. https://doi.org/10.1016/j.neuron.2018.03.032.
79. Dufour, A., Meas-Yedid, V., Grassart, A., and Olivo-Marin, J.-C. (2008). Automated quantification of cell endocytosis using active contours and wavelets. In 2008 19th International Conference on Pattern Recognition (IEEE), pp. 1–4. https://doi.org/10.1109/ICPR.2008.4761748.

STAR★METHODS

KEY RESOURCES TABLE

REAGENT or RESOURCE	SOURCE	IDENTIFIER
Antibodies		
Atto647N FluoTag®-X4 anti-RFP	NanoTag	Cat#N0404-Atto647-NL
Chemicals, Peptides, and Recombinant Proteins		
4-methylcyclohexanol (98%)	Sigma-Aldrich	Cat# 218405
3-octanol (99%)	Sigma-Aldrich	Cat# 153095
Paraffin oil	VWR	Cat#24679
D-Trehalose dihydrate	Sigma-Aldrich	Cat#T9531
Sucrose	Sigma-Aldrich	Cat#S9378
NaCl	Sigma-Aldrich	Cat#S9625
KCl	Sigma-Aldrich	Cat#P3911
$CaCl_2$	Sigma-Aldrich	Cat#C3881
$MgCl_2$	Sigma-Aldrich	Cat#M9272
Hepes-hemisodium salt	Sigma-Aldrich	Cat#H7637
Sodium Azide	Sigma-Aldrich	Cat#71289
Prolong Mounting Medium	Lifetechnology	Cat#P36930
BSA	Sigma-Aldrich	Cat#A9085
Critical commercial assays		
RNeasy Plant Mini Kit	QIAGEN	Cat. #74904
RNA MinElute Cleanup Kit	QIAGEN	Cat. #74204
SuperScript III First-Strand Kit	Thermofisher Invitrogen	Cat. #18080-051
SYBR Green I Master mix	Roche	Cat. # 04729692001
Experimental Models: Organisms/Strains		
VT30559-Gal4	VDRC	VDRC 206077
tub-Gal80^{ts}	BDSC	BDSC 7019
c739-Gal4	BDSC	BDSC 7362
VT30604-Gal4	VDRC	VDRC 200228
VT49483-Gal4	VDRC	VDRC 206419
tub-Gal80^{ts}	BDSC	BDSC 7019
tub-Gal80^{ts}; VT30559-Gal4	Plaçais et al.[34]	N/A
tub-Gal80^{ts}; c739-Gal4	Turrel et al.[75]	N/A
tub-Gal80^{ts}; VT30604-Gal4	Turel et al.[75]	N/A
tub-Gal80^{ts}; VT49483-Gal4	Turel et al.[75]	N/A
UAS-mt-dsRed	BDSC	BDSC 93056
UAS-Miro RNAi JF02775	BDSC	BDSC 27695
UAS-Milton RNAi JF03022	BDSC	BDSC 28385
UAS-Milton RNAi HMC02365	BDSC	BDSC 44477
UAS-OPA1 HMS00349	BDSC	BDSC 32358
UAS-Vimar HMS02397	BDSC	BDSC 41996
UAS-Vimar HMS0745	BDSC	BDSC 32951
UAS-Pink1 HMS01707	BDSC	BDSC 38262
UAS-Miro RNAi VSH330334	VDRC	VDRC v330334
UAS-OPA1 VSH330266	VDRC	VDRC v330266
UAS-Parkin KK107919	VDRC	VDRC 104363
tub-GAL80^{ts}; VT30559-Gal4, UAS-Pyronic	Plaçais et al.[34]	N/A
Mb-dsRed	Riemensperger et al.[63]	N/A

(*Continued on next page*)

CellPress
OPEN ACCESS

Continued

REAGENT or RESOURCE	SOURCE	IDENTIFIER
Mb-dsRed; VT30559-Gal4	This paper	N/A
UAS-mt-dsRed, UAS-Miro RNAi JF02775	This paper	N/A
UAS-mt-dsRed, UAS-Milton RNAi HMC02365	This paper	N/A
UAS-mt-dsRed, UAS-Miro RNAi VSH330334	This paper	N/A
UAS-mt-dsRed, UAS-Milton RNAi JF03022	This paper	N/A
Oligonucleotides		
Primers for Miro (JF02775 RNAi): Forward: AAAAGCACCTCATTCTGCGT	This paper	N/A
Primers for Miro (JF02775 RNAi): Reverse: AGTCGTAGACTAGGCAGGCA	This paper	N/A
Primers for Miro (VSH330334 RNAi): Forward: GCCCACCAGCATAGTTGACTT	This paper	N/A
Primers for Miro (VSH330334 RNAi): Reverse: CGTGCGCCTTGTTAATTTCGG	This paper	N/A
Primers for Vimar (HMS00745 and HMS02397 RNAi): Forward: TGGCAGAGTGCTTTCTGGG	This paper	N/A
Primers for Vimar (HMS00745 and HMS02397 RNAi): Reverse: ACTTGGTGATCTCCGCAATGC	This paper	N/A
Primers for OPA1 (VSH330266 and HMS00349 RNAi): Forward: CGAGAAAAGCTGTTGTCTACTCC	This paper	N/A
Primers for OPA1 (VSH330266 and HMS00349 RNAi): Reverse: GATGGCTGGTGATGCCACA	This paper	N/A
Primers for Parkin (KK107919 RNAi): Forward: AGCGATGCCACGACAATAGAGC	Sun et al.[61]	N/A
Primers for Parkin (KK107919 RNAi): Reverse: GCGAAGGTTCCTCCTCCTCCAA	Sun et al.[61]	N/A
Primers for α-Tub84B: Forward: TTGTCGCGTGTGAAACACTTC	Turrel et al.[75]	N/A
Primers for α-Tub84B: Reverse: CTGGACACCAGCCTGACCAAC	Turrel et al.[75]	N/A
Software and Algorithms		
GraphPad Prism 5	GraphPad Software Inc. Press, San Diego CA, 2007	http://www.graphpad.com/ RRID:SCR_002798
Matlab V2013	The Mathworks Inc., Natick, MA	https://fr.mathworks.com/ RRID:SCR_001622
Fiji	NIH	https://imagej.net/Fiji RRID:SCR_002285
Icy	de Chaumont et al.[76]	https://icy.bioimageanalysis.org RRID:SCR_010587
Macro Minimal envelope	This paper	https://doi.org/10.5281/ZENODO.7118602

RESOURCE AVAILABILITY

Lead contact

Further information and requests for resources and reagents should be directed to and will be fulfilled by the lead contact, Pierre-Yves Plaçais (pierre-yves.plaçais@espci.fr).

Materials availability

Materials generated in this study are available from the lead contact without restriction.

Data and code availability

To determine the volume of the minimal envelope containing all of the mitochondria in each analyzed ROI, a custom macro was designed in Fiji, available on Zenodo at Minimal Enveloppe Estimation | Zenodo.[59] All data needed to evaluate the conclusions are

present in the manuscript and/or the supplemental information. Data reported in this paper will be shared by the lead contact upon request. Any additional information required to reanalyze the data reported in this paper is available from the lead contact upon request.

EXPERIMENTAL MODEL AND SUBJECT DETAILS

D. melanogaster flies were raised on standard food medium containing yeast, cornmeal and agar, on a 12 h:12 h light–dark cycle at 18°C with 60% humidity. Both male and female flies were used for behavior experiments. Female flies were used for imaging experiments due to their larger size. All fly stocks used are listed in the key resources table. Flies from the Vienna Drosophila Resource Center (VDRC) collection were outcrossed for 5 generations to a reference strain carrying the w^{1118} mutation in an otherwise Canton Special (Canton S) genetic background. Since TRiP RNAi transgenes are labeled with a y^+ marker, flies from the TRiP RNAi collection were outcrossed to a y^1w^{67c23} strain in an otherwise Canton S background. The Canton S strain was used as the wild type strain. The VT30559-Gal4 line was used for transgene expression in MB neurons, the c739-Gal4 line for expression in α/β neurons, the VT30604-Gal4 for expression in α'/β' neurons and the VT49483-Gal4 for expression in γ neurons. To restrict UAS/GAL4-mediated expression to the adult stage, we used the TARGET system with the tubulin-Gal80^{ts} (tub-Gal80^{ts}) line as described in ref. Musso et al.[77] The tub-Gal80^{ts}; VT30559-Gal4 inducible driver line was constructed in the laboratory and described in ref. Plaçais et al.[34] as well as the tub-Gal80^{ts}; c739-Gal4 line, tub-Gal80^{ts}; VT30604-Gal4 line and the tub-Gal80^{ts}; VT30559-Gal4 line described in ref. Turrel et al.[75] Gal4 activity was released by transferring 0- to 2-day-old adult flies to 30°C for 3 d. The tub-GAL80^{ts}; VT30559-GAL4, UAS-Pyronic line was previously generated in our research group and described in ref. Plaçais et al.,[34] while the UAS-mt-dsRed, UAS-Miro RNAi JF02775 line, the UAS-mt-dsRed, UAS-Miro RNAi VSH330334 line, the UAS-mt-dsRed, UAS-Milton RNAi HMC02365 line and the UAS-mt-dsRed, UAS-Milton RNAi JF03022 line were generated for this study.

METHOD DETAILS

Olfactory conditioning and memory test

The behavioral experiments, including sample sizes, were conducted similarly to previous studies from our research group.[34,78] For all experiments, training and testing were performed at 25°C and 80% humidity. For olfactory conditioning protocols, groups of 20-40 flies were subjected to either a single cycle (1x training), five associative cycles spaced by 15-min inter-trial intervals (5x spaced training) or five consecutive associative cycles (5x massed training). Non-associative control protocols (unpaired protocols) were also used for imaging and immunohistochemistry experiments. Conditioning was performed using previously described barrel-type machines that allow the parallel training of up to 6 groups. Throughout the conditioning protocol, each barrel was plugged into a constant air flow at 2 L.min-1. For a single cycle of associative training, flies were first exposed to an odorant (the CS+) for 1 min while 12 pulses of 60 V electric shocks (1 pulse every 5s, pulse duration 1.2s) were delivered; flies were then exposed 45 s later to a second odorant without shocks (the CS-) for 1 min. The odorants 3-octanol and 4-methylcyclohexanol, diluted in paraffin oil to a final concentration of $2.79 \cdot 10^{-1}$ g.L^{-1}, were alternately used as conditioned stimuli. During unpaired conditionings, the odor and shock stimuli were delivered separately in time, with shocks starting 3 min before the first odorant. Flies were kept on standard medium between conditioning and the memory test, either at 25°C for flies tested 3 h after training or at 18°C for flies tested 24 h after training. The memory test was performed in a T-maze apparatus, typically 3 h after single-cycle training or 24 h after spaced training (except for Figure S1A) or massed training. Each arm of the T-maze was connected to a bottle containing 3-octanol and 4-methylcyclohexanol, and diluted in paraffin oil to a final concentration identical to the one used for conditioning. Flies were given 1 min to choose between either arm of the T-maze, after which they were trapped, collected, and counted. A performance score was calculated as the number of flies avoiding the conditioned odor minus the number of flies preferring the conditioned odor, divided by the total number of flies. A single performance index value is the average of two scores obtained from two groups of genotypically identical flies conditioned in two reciprocal experiments, using either odorant (3-octanol or 4-methylcyclohexanol) as the CS+. The indicated 'n' is the number of independent performance index values for each genotype.

The shock response tests were performed at 25°C by placing flies in two connected compartments; electric shocks were administered in only one of the compartments. Flies were given 1 min to move freely in these compartments, after which they were trapped, collected, and counted. The compartment in which the electric shocks were delivered was alternated between two consecutive groups. Shock avoidance was calculated as for the memory test. Since the delivery of electric shocks can modify olfactory acuity, our olfactory avoidance tests were performed on flies that had first been presented another odor paired with electric shocks. Innate odor avoidance was measured in a T-maze similar to those used for memory tests, in which one arm of the T-maze was connected to a bottle with odor diluted in paraffin oil and the other arm was connected to a bottle with paraffin oil only. Naive flies were given the choice between the two arms during 1 min. The odor-interlaced side was alternated for successively tested groups. Odor concentrations used in this assay were the same as for the memory assays. At these concentrations, both odorants are innately repulsive.

Confocal imaging of mitochondria in naive flies

To assess the effect of the Miro or Milton RNAi lines on overall mitochondria distribution in the MB of naive flies, tub-GAL80^{ts}; VT30559-GAL4 flies were crossed with flies bearing UAS-mt-dsRed with or without the UAS-RNAi, and raised at 18°C. To achieve the induction of RNAi expression and mt-dsRed, F1 adult flies were kept at 30.5°C for 3 d before dissection. Whole adult flies were

fixed in 4% paraformaldehyde (Electron Microscopy Sciences) in PBST (PBS containing 0.6% Triton X-100) at 4°C overnight. Next, brains were dissected in PBS solution and directly mounted using ProLong Gold Antifade Mountant (Invitrogen). Acquisitions were made the following day with a Nikon A1R confocal microscope with a 20x objective.

Immunostaining for STED microscopy

For immunostaining experiments, flies were raised at 18°C. To achieve the induction of RNAi expression and mt-dsRed, adult flies were kept at 30.5°C for 3 d before conditioning with either 5x spaced training or one-cycle training. One hour after the end of the training period, whole adult flies were fixed in 4% paraformaldehyde (Electron Microscopy Sciences) in PBST (PBS containing 0.6% Triton X-100) at 4°C overnight. Next, brains were dissected in PBS solution and fixed again for 1 h at room temperature (RT) in 4% paraformaldehyde in PBST followed by three 20-min rinses in PBST, with blocking for 2 h at RT with 2% BSA (Sigma-Aldrich cat#A9085) in PBST. Samples were incubated with the primary antibody Atto647N FluoTag®-X4 anti-RFP (NanoTag cat#N0404-Atto647N-L) at 1:100 in the blocking buffer at 4°C overnight. The next day, brains were rinsed twice for 20 min in PBST and once for 20 min in PBS. Samples were then mounted in ProLong Gold Antifade Mountant (Invitrogen) using precision cover glasses with thickness No. 1.5H (Marienfeld Superior).

Image acquisition and analysis of immunostaining

Single-color 3D-STED imaging was performed using a Leica TCS SP8 STED 3X microscope (excitation at 633 nm, STED depletion laser at 775 nm (pulsed), with 60% in x and y dimensions and 50% in z dimension) with a 93x motCorr glycerol immersion objective (NA=1.3). Images of one MB soma region per brain were obtained with a voxel size of 41.68 nm (x) x 41.68 nm (y) x 72.48 nm (z). For soma analysis, one ROI per brain containing only soma was delimited from the full image (120 μm x 120 μm x 8 μm) using a constant square box of 21 μm x 21 μm x 8 μm. The raw ROIs were then analyzed using Icy Software and the HK-mean plugin followed by the connected-component (ROI extraction mode, removal of the border objects) plugin to detect mitochondria and their volumes.[76,79] Each ROI typically contained around 250-300 mitochondria. The same parameters (i.e. the Gaussian pre-filter and the intensity classes) were used for all ROIs analyzed in the study. These parameters were first determined on a set of ROIs from brain samples by a researcher blind for the genotype and the behavioral training. The volume of the minimal envelope containing all of the detected mitochondria in each ROI was determined using a custom-written ImageJ macro.[59] Briefly, we proceeded with the binarization of single fluorescent images of the z-stack series obtained from the Icy analysis. Binarized fluorescent objects were then connected using XOR and Convex Hull mathematical operators. Surface and volume estimates were performed using the 3D object option available in Fiji.

The full z-stacks that we acquired were centered on the soma region, but they included a portion of the calyx embedded within neuronal somas, which we used to analyze mitochondria content in the dendritic compartment, albeit with a reduced ROI due to the reduced z-thickness of the recorded calyx area. The ROI surface was increased and adjusted to the shape of the calyx (a round ROI of 31 μm diameter and 2.3 μm thickness was used). The same brains were used for soma and calyx analyses. The raw ROIs were then analyzed using the same process and parameters as for soma ROI. Due to the smaller ROI size, and to avoid discarding too many objects located at the borders, we chose not to remove the border objects (in all directions) in the connected-component analysis, which may result in misestimating the absolute mitochondria total density and volume of the largest mitochondria (which are more likely to be cropped). Because of these limitations, comparisons between mitochondria density in the soma and the calyx should be avoided, and we only compared data within the calyx between different conditioning protocols.

Based on the distribution of mitochondria volume in the control group (5x spaced unpaired, tub-Gal80^{ts}>UAS-mt-dsRed), we defined 4 categories of mitochondria, from the smallest volume to the largest, using the mean of the 25th and 75th percentiles and the medians of mitochondria volumes in each ROI from one fly brain (Figure 2D). The limit of each category is defined as follows: for category 1 (the smallest), the upper limit is the mean of the 25th percentiles; for category 2, the lower limit is the mean of the 25th percentiles and the upper limit is the mean of the medians; for category 3, the lower limit is the mean of the medians and the upper limit is the mean of the 75th percentiles; and for category 4 (the largest), the lower limit is the mean of the 75th percentiles. The same volume limits were used to define the categories in all experimental conditions. Then, to allow comparisons between the samples, for each ROI from one fly brain, we normalized the number of mitochondria in each category by the volume of the minimal envelope containing all of the detected mitochondria, in order to obtain a density of mitochondria for each category (Figure 2D; Video S3 and ref. Bun[59] for the Fiji custom-written macro).

Confocal imaging of the entire MB shown in Figure 2B was conducted on one sample used for 3D-STED imaging, and was performed on the same Leica TCS SP8 microscope used for 3D-STED imaging. Images of an entire MB were obtained with a voxel size of 120 nm (x) x 120 nm (y) x 330 nm (z).

In vivo imaging

For imaging experiments, flies were raised at 23°C to increase the expression level of genetically encoded sensors. To achieve the induction of RNAi expression, adult flies were kept at 30.5°C for 3 days before conditioning. As in all previous imaging work from our laboratory, all *in vivo* imaging was performed on female flies, which are preferred since their larger size facilitates surgery. A single fly was picked and prepared for imaging as previously described.[34] Briefly, the head capsule was opened and the brain was exposed by gently removing the superior tracheae. For the duration of the preparation, the head capsule was bathed in an artificial hemolymph

solution composed of NaCl 130 mM (Sigma cat. # S9625), KCl 5 mM (Sigma cat. # P3911), $MgCl_2$ 2 mM (Sigma cat. # M9272), $CaCl_2$ 2 mM (Sigma cat. # C3881), D-trehalose 5 mM (Sigma T cat. # 9531), sucrose 30 mM (Sigma cat. # S9378), and HEPES hemisodium salt 5 mM (Sigma cat. # H7637). At the end of surgery, any remaining solution was absorbed and a fresh 90-μL droplet of this solution was applied on top of the brain.

Pyruvate imaging

Pyruvate imaging experiments were performed using the tub-GAL80^{ts}; VT30559-GAL4, UAS-Pyronic line generated in ref. Plaçais et al.[34] along with the appropriate RNAi line. Data were collected indiscriminately from 30 min to 1.5 h after 5x spaced training or 1x training.

Two-photon imaging was performed using a Leica TCS-SP5 upright microscope equipped with a 25x, 0.95 NA water immersion objective. Two-photon excitation was achieved using a Mai Tai DeepSee laser tuned to 825 nm. The frame rate was set to 2 images per second. Pyruvate consumption measurements were performed according to a previously well-characterized protocol.[34] After 1 min of baseline acquisition, 10 μL of a 50 mM sodium azide solution (Sigma cat. #71289; prepared in the same artificial hemolymph solution) were injected into the 90-μL droplet bathing the fly's brain, bringing sodium azide to a final concentration of 5 mM. To analyze the pyruvate imaging experiments, ROI were delimited by hand around each visible MB neuronal compartment of interest (ie either the vertical lobe, the soma, the calyx, or the horizontal lobe) and the average intensity of the mTFP and Venus channels over each ROI was calculated over time after background subtraction. The Pyronic sensor was designed so that FRET from mTFP to Venus decreases when the pyruvate concentration increases. To obtain a signal that positively correlates with pyruvate concentration, the inverse FRET ratio was computed as mTFP intensity divided by Venus intensity. This ratio was normalized by a baseline value calculated over the 30 s preceding drug injection. The slope was calculated between 10 and 70% of the plateau. We previously demonstrated that the slope of pyruvate accumulation in the cytosol is an accurate way to measure pyruvate flux to the mitochondria, as cytosolic pyruvate accumulation was directly related to the level of mitochondrial pyruvate oxidation by the Pyruvate Dehydrogenase complex[34] The indicated 'n' is the number of animals that were assayed in each condition and an independent set of experiments were done for each neuronal compartment.

FRAP experiment

FRAP experiments were performed using the F1 from either MB-dsRed, VT30559-Gal4 line crossed with CS, or the tub-Gal80^{ts}; VT30559-Gal4 line crossed with the UAS-mt-dsRed with or without the UAS-RNAi. Data recording started 30 min after 5x spaced training.

FRAP experiments were performed using a Leica TCS-SP5 upright microscope equipped with a 25x, 0.95 NA water immersion objective. Excitation was achieved using an argon laser (514 nm) pre-set at 80% of its maximal power. After one z-stack of baseline acquisition (e.g. the z-stack beginning above the vertical lobes, down to the junction area with the horizontal lobes, with a z-step of 1.48 μm), we switched to the FRAP module of the LAS-AF software, which allows bleaching on a selected confocal plane corresponding to the tip of the α lobe. This bleaching was only performed on one hemisphere. The following parameters were used for the bleaching time series: pre-bleach acquisition (laser line: 514 nm, intensity: 3%, frequency: 1 frame per 10 s, 3 frames), bleaching (laser line: 514 nm, intensity: 100%, frequency: 1 frame per 0.648 s, 20 frames), post-bleaching acquisition (laser line: 514 nm, intensity: 3%, frequency: 1 frame per 10 s, 5 frames). Then, when switching back to classical acquisition mode, the recovery of fluorescence was recorded during 60 min by acquiring z-stacks at a frequency of 1 frame/5 min (except for the cytoplasmic dsRed recording, for which the frequency of acquisition was increased to 1 frame/2.5 min). To analyze the FRAP experiments, ROI (one per brain) were delimited by hand corresponding to the bleached region (the tip of the vertical lobe), and the average dsRed fluorescence intensity (F_t) was calculated over time after background subtraction. To control for any z-deviation that could occur during the 60-min long recording, a non-bleached region from the other hemisphere was used as a landmark. The Fluorescence Recovery Index corresponds to F_t-F_0/$F_{initial}$, in which F_t is the fluorescence over time, F_0 is the fluorescence immediately after bleaching (i.e. the mean of the fluorescence measured on the 5 frames collected within 1 min after bleaching), and $F_{initial}$ is the fluorescence before bleaching (i.e. the mean of the fluorescence from the first acquisition and the 3 pre-bleaching frames). To quantify the recovery of fluorescence, a slope measurement was made within the time interval when the fluorescence recovery index is linear as a function of time. This time interval was therefore set depending on the genotype: for a fast kinetic of Fluorescence Recovery Index (such as for cytosolic dsRed) 10-min post-bleaching was used, whereas for mitochondrial dsRed: tub-Gal80^{ts}; VT30559>UAS-mt-dsRed, UAS-Milton RNAi HMC02365 flies had a time interval of 20 min after bleaching, while tub-Gal80^{ts}; VT30559>UAS-mt-dsRed, UAS-Miro RNAi JF02775 flies and tub-Gal80^{ts}; VT30559>UAS-mt-dsRed flies had an interval of 40 min. The indicated 'n' is the number of animals that were assayed in each condition.

qPCR validation of RNAi lines

To assess the efficiency of each RNAi line used in this study (except for Milton JF03022 and Milton HMC02365, which were previously assessed in ref. Iijima-Ando et al.,[44] Liu et al.,[45] and Vagnoni et al.[46]), female flies carrying the elav-Gal4 pan-neuronal driver were crossed with the specified UAS-RNAi males, or with CS males for controls. Whenever the cross with the constitutive elav-Gal4 driver was lethal for the progeny, female flies carrying the inducible tub-Gal80^{ts}; elav-Gal4 pan-neuronal driver were used. Fly progeny were raised at 25°C throughout their development except when the inducible driver was used. These latter crosses were raised at 18°C and the adult progeny were induced for 3 days at 30°C. RNA extraction, DNAse I treatment and cDNA synthesis were performed as previously in ref. Silva et al.[64] using the RNeasy Plant Mini Kit (Qiagen), RNA MiniElute Cleanup Kit (Qiagen), DNAse I treatment (BioLabs), oligo(dT)20 primers and the SuperScript III First-Strand kit (Thermo Fisher Invitrogen). Amplification was performed using

a LightCycler 480 (Roche) and the SYBR Green I Master mix (Roche). Specific primers used for each gene cDNA and the reference α-Tub84B (Tub, CG1913) cDNA are listed in the key resources table (in the case of Miro, due to the RNAi sequence, different pairs of primers had to be designed for the same cDNA)

A-3' (ref. Sun et al.[61]);

The level of the target cDNA was compared against the level of the α-Tub84B reference cDNA. Each reaction was performed in triplicate. The specificity and size of amplification products were assessed by melting curve analyses. Expression relative to the reference was presented as the foldchange compared to the calibrator (relative quantification $RQ = 2^{-\Delta\Delta Ct}$, where Ct is the cycle threshold).

QUANTIFICATION AND STATISTICAL ANALYSIS

Statistical parameters including the definitions and exact value of n, deviations, and P values are reported in the figures and corresponding legends. Data are expressed as the mean ± SEM with dots as individual values corresponding to either: two reciprocal groups of 20–40 flies analyzed in behavioral assay; the response of a single recorded fly for pyruvate imaging and FRAP experiments; or the mitochondria density of one fly brain in STED experiments. Statistical analysis was performed using GraphPad Prism 8.0. Comparisons between two groups were performed by unpaired two-sided Student's t-test, with results given as the value tx of the t-distribution, where x is the number of degrees of freedom (for pyruvate imaging, FRAP and STED experiments as well as for qPCR experiments in Figures 2E, 2F, 2G, 3B, 3C, 4B–4H, S1H, S1I, S2A–S2F, S2I, S2K, S2N–S2Q, and S3). Comparisons among three genotypic groups were performed by one-way ANOVA with post hoc testing using the Newman–Keuls pairwise comparisons test between the experimental group and its controls (significance is indicated when $P < 0.05$; all behavior experiments and some qPCR experiments in Figures 1B–1E S1A, S1E–S1G, S1L–S1Q, S2H, S2J, S2L, and S2M and Tables 1 and S1). ANOVA results are given as the value of the Fisher distribution F(x,y), where x is the number of degrees of freedom numerator and y is the total number of degrees of freedom denominator. Asterisks in each figure refer to the least significant post hoc comparison between the genotype of interest and the genotypic controls. The nomenclature used corresponds to *$P < 0.05$, **$P < 0.01$, ***$P < 0.001$, ****$P < 0.0001$ and ns: not significant, $P > 0.05$. Figures were created using Affinity Designer.